

Evaluating the skill of high resolution WRF-Chem simulations in describing drivers of aerosol direct climate forcing at the regional scale

~~How skillfully can we simulate drivers of aerosol direct climate forcing at the regional scale?~~

P. Crippa¹, R. C. Sullivan², A. Thota³, S. C. Pryor^{2,3}

[1] COMET, School of Civil Engineering and Geosciences, Cassie Building, Newcastle University, Newcastle upon Tyne, NE1 7RU, UK

[2] Department of Earth and Atmospheric Sciences, Bradfield Hall, 306 Tower Road, Cornell University, Ithaca, NY 14853, USA

[3] Pervasive Technology Institute, Indiana University, Bloomington, IN 47405, USA

Correspondence to: P. Crippa (paola.crippa@ncl.ac.uk)

Abstract

Assessing the ability of global and regional models to describe aerosol optical properties is essential to reducing uncertainty in aerosol direct radiative forcing in the contemporary climate and to improving confidence in future projections. Here we evaluate the skill-performance of high-resolution simulations conducted using the Weather Research and Forecasting model with coupled chemistry (WRF-Chem) in capturing spatio-temporal variability of aerosol optical depth (AOD) and Ångström exponent (AE) by comparison with ground- and space- based remotely sensed observations. WRF-Chem is run over eastern North America at a resolution of 12 km for a representative year (2008). A ~~small~~-systematic positive bias in simulated AOD relative to observations is found (annual MFB=0.175 and 0.50 when comparing with MODIS and AERONET respectively), whereas the spatial variability is well captured during most months. The spatial correlation of observed and simulated AOD shows a clear seasonal cycle with highest correlation during summer months ($r=0.5-0.7$) when the aerosol loading is large

and more observations are available. ~~AE is retrieved with higher uncertainty from the remote sensing observations.~~ The model is biased towards simulation of coarse mode aerosols (annual MFB for AE = -0.10 relative to MODIS and -0.59 for AERONET), but the spatial correlation for AE with observations is 0.3-0.5 during most months, despite the fact that AE is retrieved with higher uncertainty from the remote sensing observations. WRF-Chem also exhibits high skill in identifying areas of extreme and non-extreme aerosol loading, and its ability to correctly simulate the location and relative intensity of ~~an~~ extreme aerosol events (i.e. AOD>75th percentile) varies between 30 and 70% during winter and summer months respectively.

1. Introduction and Objectives

Atmospheric aerosol particles (aerosols) play a major role in dictating Earth's climate by both directly interacting with solar radiation (direct effect) and acting as cloud condensation nuclei and thus changing cloud properties (indirect effect) (Boucher et al., 2013). The global mean aerosol direct effect is estimated to be -0.27 (possible range of -0.77 to +0.23) W m⁻², while the indirect effect is -0.55 (-1.33 to -0.06) W m⁻² (Stocker et al., 2013). Therefore their combined radiative forcing is likely a significant fraction of the overall net anthropogenic climate forcing since pre-industrial times (i.e. 1.13-3.33 W m⁻² (Stocker et al., 2013)) and a substantial source of uncertainty in quantifying anthropogenic radiative forcing.

Accurate quantification of direct aerosol radiative forcing is strongly dependent on aerosol precursor and primary aerosol emissions. Both have evolved over the past two decades in terms of their spatio-temporal distribution and absolute magnitude. Emissions have generally increased in emerging economies (Kurokawa et al., 2013), biogenic and anthropogenic emissions have altered in response to changing land use and land cover (Wu et al., 2012), and the implementation of pollution control strategies particularly in North America and Europe have resulted in declines in air pollutant emissions (Xing et al., 2015; Giannouli et al., 2011). Therefore there is evidence that aerosol burdens and thus direct climate forcing has varied markedly in the past and may change substantially in the future. Further, although best estimates of global anthropogenic radiative forcing from the aerosol direct and indirect effect are -0.27 and -0.55 W m⁻² (Stocker et al., 2013) respectively, the short residence time and high spatio-temporal variability of aerosol populations mean their impact on regional climates can be much larger than the global mean but are even more uncertain.

Long-term measurements of aerosol properties are largely confined to aerosol mass (total, PM₁₀ or PM_{2.5}) in the near-surface layer which may or may not be representative of either the total atmospheric burden (Ford and Heald, 2013;Alston et al., 2012), or radiation extinction and hence climate forcing. Further, aerosol composition measurements are often a 24-hour integrated sample taken only 1 in 3 days and thus are subject to under sampling. Hence they provide an incomplete description of temporal variability and mean aerosol burdens for model performance evaluation. ~~Long-term continuous and high precision measurements of aerosol properties are largely confined to aerosol mass (total, PM₁₀ or PM_{2.5}) in the near-surface layer which may or may not be representative of either the total atmospheric burden (Ford and Heald, 2013;Alston et al., 2012), or radiation extinction and hence climate forcing.~~ Columnar remote sensing measurements of aerosol optical properties are available from a range of ground-based and satellite-borne instrumentation, but have only a relatively short period of record, are subject to non-zero measurement uncertainty (and bias), and under-sample the range of atmospheric conditions due to cloud masking and infrequent satellite overpasses. Therefore, regional and global models are most commonly used to quantify historical and contemporary aerosol direct radiative forcing based on simulated properties such as the aerosol optical depth (AOD) and Ångström exponent (AE) (Boucher et al., 2013).

Most global models that include aerosol microphysics have been run at fairly coarse resolution (spatial resolution of the order of 1-2.5°) (Table 1) usually for periods of a few years. The resulting fields of AOD (and less frequently AE) have been evaluated relative to ground-based and satellite-borne remote sensing optical properties measurements (Table 1). However, aerosol populations (and dynamics) are known to exhibit higher spatial variability (and scales) than can be manifest in those models (Kovacs et al.,2006;Kulmala et al., 2011;Santese et al., 2007; Schutgens et al., 2013;Sinzuka and Redemann, 2011). ~~However, aerosol populations (and dynamics) are known to exhibit higher spatial variability (and scales) than can be manifest in those models (Kulmala et al., 2011;Spracklen et al., 2010).~~ Despite recent improvements in the sophistication of aerosol processes and properties within global models, there are still substantial regional and latitudinal discrepancies in both the magnitude of AOD and other aerosol properties which impact aerosol direct radiative forcing and the degree of model-to-model agreement (Myhre et al., 2013). Thus the skill of these models in reproducing the spatio-temporal variability in the aerosol size distribution, composition, concentration and radiative properties is incompletely characterized. Further large model-to-model variability both in the global mean direct aerosol forcing and in the spatial distribution thereof exists (Kulmala et al.,

2011;Myhre et al., 2013) leading to high uncertainty in quantification of aerosol climate forcing. The skill of these models in reproducing the spatio-temporal variability in the aerosol size distribution, composition, concentration and radiative properties is incompletely characterized. Accordingly, there is large model-to-model variability both in the global mean direct aerosol forcing and in the spatial distribution thereof (Kulmala et al., 2011;Myhre et al., 2013). Although a direct comparison between the studies summarized in Table 1 is inherently very difficult due to the different performance metrics reported, and variations in both the model resolution and aerosol descriptions, there is a consistent finding of high spatial variability in model bias, both in sign and magnitude. Correlation coefficients of monthly and seasonal mean AOD from model simulations versus satellite-based measurements are typically in a range ~0.6-0.8 both in global (Colarco et al., 2010;Lee et al., 2015) and regional (Nabat et al., 2015) simulations. However, these correlations are largely reflective of the ability of the models to capture the seasonal cycle and columnar aerosol properties from remote sensing and thus ignore substantial variability on the synoptic (Sullivan et al., 2015) and meso-scales (Anderson et al., 2003). A wider range of correlation coefficients are reported when comparisons are made to high frequency observations of AOD at the hourly/daily timescale both in global (Sič et al., 2015) and regional (Rea et al., 2015) simulations ($r \sim 0.3-0.8$). The largest range of correlation coefficients ($[-0.99, 0.9]$; Table 1) is reported when simulated AOD is compared with observations from the AErosol RObotic NETwork (AERONET), and appear to be function of temporal averaging, location of AERONET sites and model resolution. Correlations between time series of simulated AE versus AERONET observations are reported less frequently, and when conducted for monthly mean values range from ~0.4 (Li et al., 2015) to ~0.8 (Colarco et al., 2010).

At least some of the variability in model skill performance, as indicated by the mutual variability with observations described by correlation coefficients, and model-to-model agreement shown in AeroCom Phase II may be attributable to variations in model resolution, differences in gas and particle phase parameterizations and aerosol descriptions. However, there are also variations in the way in which model skill is evaluated and divergent opinions regarding prioritization of future research directions.~~However, there are also variations in the way in which model skill is evaluated leading to ambiguity in terms of prioritizing future research directions.~~ The direct effect remains poorly quantified at the regional scale, due to uncertainty in aerosol loading, uncertainty and spatio-temporal variability in aerosol physical properties (Colarco et al., 2014) and a relative paucity of rigorous model verification and validation

exercises. Confidence in projections of possible future aerosol radiative forcing requires detailed assessment of skill in the current climate, and the need for and benefits of regional downscaling and/or use of high-resolution global models requires careful quantification.

Regional models represent an opportunity to assess if running higher resolution simulations over specific regions of interest improves the characterization of aerosol optical properties of relevance to direct radiative forcing. Assessment of value added (or lack thereof) from high resolution regional versus global coarse resolution models has not been clearly quantified in previous studies (Table 1).

~~Assessment of value added (or lack thereof) from high resolution regional versus global coarse resolution models is not quantifiable from prior studies alone.~~ Although high-resolution simulations, comparable to those presented herein, have been run, they are over a small temporal and spatial domain (e.g. (Tuccella et al., 2015)), or lack quantitative assessment of aerosol optical properties (e.g. (Tessum et al., 2014)). Thus, quantification of the skill of high-resolution modeling of aerosol optical properties is presented here along with a preliminary analysis of model performance as a function of spatial aggregation. Forthcoming work will include direct comparison to coarser resolution simulations to quantify the value added (or lack thereof) from increased model resolution.

We evaluate the skill of state-of-the-art high-resolution regional model simulations of climate-relevant aerosol properties using a range of ~~inferential-descriptive~~ statistics and investigate possible sources of discrepancies with observations. The impact of aerosols on climate and human health are strengthened under conditions of enhanced aerosol concentrations, thus it is necessary to study and diagnose causes of ‘extreme aerosol events’ (Chu, 2004; Gkikas et al., 2012), and to evaluate the ability of numerical models to simulate their occurrence, intensity, spatial extent and location. Prior analyses of Level-3 (1° resolution) MODIS AOD over the eastern half of North America have indicated ~~the frequency of co-occurrence of~~ extreme AOD values (> local 90th percentile) are coherent over ~~decreases to below 50% at regional scales (~ 150 km) from a central grid cell located in southern Indiana, but is above that expected by random chance over almost all of eastern North America~~ (Sullivan et al., 2015). Thus, our evaluation exercise also includes an analysis of the spatio-temporal coherence of extreme events.

We applied the Weather Research and Forecasting model with coupled Chemistry (WRF-Chem version 3.6.1) at high resolution (12×12 km) over eastern North America during the year 2008, in the context of a pseudo type-2 downscaling exercise in which the high-resolution model is

nested within reanalysis boundary conditions (Castro et al., 2005). The choice of this spatial resolution is taken in part to match the resolution of North American Mesoscale Model that is used for the meteorological lateral boundary conditions and to ensure we capture some mesoscale variability while remaining computationally feasible.

Our evaluation is designed to investigate spatio-temporal variability of aerosol optical properties (i.e. AOD and AE) in their mean and extreme values. Thus, we conduct our evaluation of the simulations using:

- (i) High-frequency, disjunct time series data from ~~columnar~~-point measurements at AERONET stations.
- (ii) Relatively high-resolution spatial data from lower frequency (once daily or lower) data from polar orbiting satellites (i.e. MODIS and MISR).

We also include intercomparison with daily mean PM_{2.5} concentrations from 1230 surface stations and near-surface PM_{2.5} composition using data from 123 IMPROVE sites. The PM_{2.5} concentrations ~~se~~-data for 2008 were obtained from the US Environmental Protection Agency (EPA) AirData web site and represent all available outdoor near-surface 24-hour mean PM_{2.5} measurements in the model domain. Most of these stations report values on a 1 day in 3 schedule.- Daily average PM_{2.5} chemical compositions are also available on 1 day in 3 and were accessed online through the IMPROVE data wizard. We further evaluate the WRF-Chem simulations of a key meteorological parameter – precipitation – relative to observations from the Delaware gridded dataset (Matsuura and Willmott, 2009). This data set includes monthly accumulated precipitation data on a 0.5×0.5° grid which is estimated by interpolating station observations from the Global Historical Climatology Network using the spherical version of Shepard's distance-weighting method (Shepard, 1968; Willmott et al., 1985).

This paper is structured as follows. We first describe the settings used in our WRF-Chem simulations and introduce the remote sensing and other data used for model evaluation (Sect. 2). A description of statistical metrics used for the evaluation is also provided. Section 3 presents results of the evaluation of simulated AOD and AE versus observations, as well as findings on extreme AOD values. In Section 4 we summarize our findings and draw conclusions.

2. Methods

2.1 WRF-Chem simulations

The Weather Research and Forecasting Model with coupled chemistry (WRF-Chem, version 3.6.1) (Grell et al., 2005; Fast et al., 2006) is used to simulate aerosol processes over eastern North America during the whole of 2008. The simulation domain comprises 300×300 grid points with 12 km resolution and is centered in southern Indiana (86°W, 39°N). The calendar year 2008 was selected because it is representative of average climate and aerosol conditions in the center of the model domain (near Indianapolis, IN). In 2008, mean T_{\max} , T_{\min} , precipitation, and wind speed as measured at the National Weather Service Automated Surface Observing Systems (NWS ASOS) station at Indianapolis International Airport are within ± 0.25 standard deviations (σ) of the 2000-2013 seasonal means. Further, mean seasonal AOD from Level-3 MODIS retrievals is within $\pm 0.2\sigma$ of 2000-2013 mean values. Additionally, choice of this year ensures availability of multiple sources of ground- and space-based measurements of aerosol properties for evaluation of the simulations.

Table 2 provides details of the WRF-Chem simulations. In brief, we used 32 vertical levels up to 50 hPa with telescoping to allow for a good vertical resolution in the boundary layer (i.e. approximately 10 layers below 1 km for non-mountainous regions). Meteorological lateral boundary conditions are provided every 6 hours from the North American Mesoscale Model (NAM) applied at 12 km resolution. The initial and boundary chemical conditions are based on output from the offline global chemical transport model MOZART-4 (Model for Ozone and Related chemical Tracers, version 4), driven by meteorology from NCEP/NCAR-reanalysis (Pfister et al., 2011; Emmons et al., 2010). Anthropogenic emissions are from the POET (Precursors of Ozone and their Effects in the Troposphere) and the EDGAR (Emissions Database for Global Atmospheric Research) databases. The land cover is specified based on the USGS 24-category data at 3.7 km resolution (Anderson et al., 1976). Anthropogenic point and area emissions at 4 km resolution are input hourly from the U.S. National Emissions Inventory (NEI-05) (US-EPA, 2009) and specified for 19 vertical levels (see Fig. 1 for an overview of the primary aerosol emissions). Biogenic emissions of isoprene, monoterpenes, other biogenic VOC (OVOC), and nitrogen gas emissions from the soil are described as a function of simulated temperature and photosynthetic active radiation (for isoprene) using the model of Guenther (Guenther et al., 1993; Guenther et al., 1994; Simpson et al., 1995). Aerosol and gas phase chemistry are described using the second generation Regional Acid Deposition

Model (RADM2) chemical mechanism (Stockwell et al., 1990) and the Modal Aerosol Dynamics Model for Europe (MADE) which incorporates the Secondary Organic Aerosol Model (SORGAM) (Ackermann et al., 1998; Schell et al., 2001). The correct characterization of aerosol optical properties is ~~strongly related to~~ dependent on model skill in describing particle composition and mixing state (Li et al., 2015; Curci et al., 2014). With this in mind, it is worthy of note that aerosol components are assumed to be internally mixed within each mode (although the composition differs by mode). ~~For the~~ The standard deviation on the log-normal Aitken and accumulation modes the ~~median diameters are 10 nm and 70 nm with~~ standard deviations ~~of~~ are fixed at 1.6 and 2, respectively. The choice of a modal representation of aerosol size distribution is dictated by the high computational demand of more sophisticated approaches (e.g. sectional description of the aerosol size distribution) for long-term simulations. With the current settings, the 1-year run was completed without restart in 9.5 days (230 hours) on the Cray XE6/XK7 supercomputer (Big Red II) owned by Indiana University using 256 processors distributed on 8 nodes, thus indicating feasibility of this configuration for climate scale simulations. Aerosol, and gas phase concentrations and meteorological properties are saved once hourly. AE from the WRF-Chem simulations is computed using:

$$AE = \frac{\ln \frac{AOD_{400nm}}{AOD_{600nm}}}{\ln \frac{600nm}{400nm}} \quad (1).$$

AOD at wavelengths (λ) of 500 and 550 nm for comparison with MODIS and MISR respectively, are derived using the Ångström power law:

$$AOD_{\lambda} = AOD_{300} \times \frac{\lambda^{(-AE)}}{300} \quad (2).$$

We investigated the wavelength dependence on AE calculation using λ at 300 nm and 1000 nm as proposed in (Kumar et al., 2014) and found that, although AOD estimates are independent on the wavelength range selected, $AE_{400-600nm}$ is systematically lower than $AE_{300-1000nm}$. Analyses of AE reported in this study are obtained using ~~λ = wavelengths at~~ 400 and 600 nm since they are closer to those used in AE satellite retrievals.

2.2 Remotely-sensed data

Consistent with previous research (Sect. 1 and Table 1), we evaluate the WRF-Chem simulations using four primary remote sensing products – three are drawn from instruments on

the Aqua and Terra satellites, while the fourth is from ground-based radiometers operated as part of the AERONET network. The data sets are as follows:

The MODerate resolution Imaging Spectroradiometer (MODIS) instruments aboard the polar-orbiting Terra (~1030 overpass local solar time (LST)) and Aqua (~1330 LST) satellites. They have measured atmospheric aerosol optical properties since 2000 and 2002 respectively, with near-global daily coverage (Remer et al., 2005). Herein we use the Level 2 (L2; 10 km resolution) “dark-target” products of AOD at 550 nm and AE from 470 – 660 nm (Collection 5.1; (Levy et al., 2010)). The L2 AOD uncertainty is $\pm 0.05 \pm 0.15 \times \text{AOD}$ over land relative to global sun photometer measurements from AERONET; even when no spatiotemporal averaging is used in the comparison (i.e. all combinations of MODIS retrievals within 30 km of an AERONET site and all AERONET retrievals within 30 min of the satellite overpass), 71% of MODIS retrievals fall within a $\pm 0.05 \pm 0.2 \times \text{AOD}$ envelope relative to AERONET over E. CONUS (Hyer et al., 2011). ~~The L2 AOD uncertainty is $\pm 0.05 \pm 0.15 \times \text{AOD}$ over land relative to global sun photometer measurements from AERONET.~~ AE is retrieved with higher uncertainty, and tends to exhibit a bi-modality in retrieved values (Levy et al., 2010; Remer et al., 2005) (see ~~SM~~ Fig. S1). For this reason where we compare WRF-Chem simulated AE with values from MODIS we treat AE as a binary variable, wherein $\text{AE} < 1$ is taken as representing coarse mode dominated aerosol populations and $\text{AE} > 1$ indicates fine mode dominated populations (Pereira et al., 2011; Valenzuela et al., 2014).

2. The Multi-angle Imaging Spectroradiometer (MISR) instrument is also aboard the Terra satellite, and measures radiances at four wavelengths from 446 – 886 nm at nine viewing angles from nadir to 70.5° . MISR (L2, 17.6 km resolution) retrieves AOD with lower uncertainty than MODIS ($\pm 0.05 \times \text{AOD}$ relative to AERONET), but with lower temporal resolution (global coverage in ~ one week) (Kahn et al., 2010; Kahn et al., 2005). Herein, we use the $0.5^\circ \times 0.5^\circ$ gridded Level 3 (Ver. 31) AOD (at 555 nm) and AE (calculated from AOD at 443 and 670 nm).

3. Ground-based sun-photometer measurements from 22 AErosol RObotic NETwork (AERONET) (Holben et al., 1998) stations are also used in this study (Fig. 1). This network is highly spatially inhomogeneous, but under cloud-free conditions the observations are available at multiple times during daylight hours. AOD is measured directly by the AERONET sun photometers at seven wavelengths (340, 380, 440, 500, 670, 870, and

1020 nm) with high accuracy (i.e. AOD uncertainty of < 0.01 for $\lambda > 440$ nm (Holben et al., 2001)). The Ångström Exponent (AE) is calculated for all available wavelengths within the AOD range. The AE 870-440 nm includes the 870, 670, 500 and 440 nm AOD data. Level-2 aerosol products from AERONET (i.e. cloud screened and quality assured) have been used extensively in satellite and model validation studies (including many of those summarized in Table 1) and are used herein.

To avoid the discontinuity in the MODIS retrieval algorithm due to different assumed aerosol types (Levy et al., 2007), we confine our analyses of model skill to longitudes east of 98°W. Only WRF grid cells with cloud fraction = 0 during the satellite over pass of each grid cell are used in comparison to MODIS/MISR observations, and only grid cells with at least 5 valid observations (both from MODIS/MISR and cloud-screened WRF) during a given month are included in the analyses presented herein. ~~To avoid the discontinuity in the MODIS retrieval algorithm due to different assumed aerosol types (Levy et al., 2007), we confine our analyses of model skill to longitudes east of 98°W. All comparisons of modeled aerosol optical properties relative to MODIS observations (e.g. monthly mean values) only include grid cells for which at least 5 valid coincident observations are available during a given month after applying a cloud screen for overpass hours with cloud fraction larger than zero.~~ It is worth noting that setting a threshold of 10 observations does not significantly affect the results. For a uniform assessment, L2 MODIS and L3 MISR data have been interpolated from their native grids (and resolutions of 10 km and $0.5^\circ \times 0.5^\circ$, respectively) to the WRF-Chem 12 km resolution grid by computing the mean of pixels with valid data within $0.1^\circ/0.3^\circ$ for MODIS/MISR from the model centroids ~~0.1° (~ 20 km) from the model centroids~~. The choice of averaging over a slightly larger area than model resolution is dictated by the sparsity of valid ~~MODIS-satellite~~ retrievals. For AERONET vs. MODIS comparison, we only use the nearest MODIS data (after regridding to WRF) to each site. Where hourly WRF-Chem output is compared with data from AERONET ~~stations~~sites, a station is only included if there are at least 20 simultaneous estimates available, -and each AERONET measurement is compared to the nearest WRF-Chem time step and to the grid cell containing the station.

2.3 Statistical methods used in the model evaluation

The primary error metric of overall model performance used herein is the Mean Fractional Bias (Boylan and Russell, 2006):

$$MFB = \frac{1}{N} \sum_1^N \frac{C_m - C_0}{\frac{C_m + C_0}{2}} \quad (3).$$

MFB is a useful model performance indicator since it equally weights positive and negative biases. It varies between +2 and -2 and has a value of zero for an ideal model. Where MFB is reported for WRF-Chem versus MODIS-~~or~~ MISR/AERONET, C_m is the monthly mean AOD or AE simulated by WRF-Chem at a specific location, C_0 refers to the same quantify from MODIS or MISR remote sensing data (Table 3) and N is the sample size. ~~Where MFB is reported in comparisons of WRF-Chem with AERONET, the monthly average in the model grid cell containing the AERONET site is compared with monthly averaged observations (C_0).~~

The evaluation of WRF-Chem simulations of AOD and AE relative to satellite retrievals (MODIS and MISR) is also summarized using Taylor diagrams (Taylor, 2001) produced from the monthly means for the grid cells with simultaneous data availability. Taylor diagrams synthesize three aspects of model skill focused on evaluations of the spatial fields of the parameter of interest. The correlation coefficient of the modeled vs. observed field which is expressed by the azimuthal position, the root mean squared difference which is proportional to the distance between a point and the reference point on the x-axis (at 1, 0), and the ratio of simulated and observed spatial standard deviation which is proportional to the radial distance from the origin.

To investigate model performance at given locations through time, empirical quantile-quantile (EQQ) plots are constructed using high frequency realizations of AOD and AE at individual locations (AERONET sites) relative to WRF-Chem values simulated in the grid cell containing the measurement site. EQQ plots are thus generated for each of the AERONET stations using all hours when there are simultaneous estimates available from the direct observations and from the numerical simulations. The advantage of EQQ plots is that they make no assumptions regarding the underlying form of the data, and can be readily used to determine which parts of the modeled distribution deviate from the observations (and thus fall away from a 1:1 line).

The validity of AE estimates is a function of both the absolute magnitude of AOD and the uncertainty in the wavelength dependent AOD. AE provides information regarding the relative abundance of fine to coarse particles. Thus, here we quantify the model skill in reproducing spatial patterns of fine and coarse mode particles observed by MODIS (Terra) by comparing the frequency distribution of AE lower and higher than 1 to distinguish populations dominated

by coarse and fine aerosols respectively in WRF-Chem and MODIS (Valenzuela et al., 2014; Pereira et al., 2011). The choice of this threshold reflects the AE distribution. AE simulated by WRF-Chem generally conforms to a single normal distribution centered on 1 during January-April and on 1.3 from May-June to December; AERONET time series also tend to conform to a single mode, while MODIS estimates typically are bimodally distributed (see SM-Fig. S1). ~~A χ^2 -test is applied to assess if the frequency distribution of fine and coarse particles is the same between MODIS and WRF-Chem.~~ We therefore consider the data in the form of a contingency table (Table 4) and compute ~~the a χ^2 -test to assess if the frequency distribution of fine and coarse particles is the same between MODIS and WRF-Chem. The χ^2 statistic is applied with~~ with one degree of freedom ~~from:~~

$$\chi^2 = \sum_{i=1}^N \frac{(O_i - E_i)^2}{E_i} \quad (4)$$

~~where O_i is the frequency of observations of type i and E_i is the expected frequency of type i which is computed as the product of the row total with the column total, divided by the total number of observations. Herein we apply and a 99% confidence limit to assess significance of the χ^2 statistic.~~

As described above, the impact of aerosols on climate and human health are strengthened under conditions of enhanced aerosol concentrations, thus two analyses were undertaken to evaluate the ability of the WRF-Chem simulations to represent extreme AOD values:

1. Evaluation of the spatial patterns of extreme events. Using daily estimates of AOD in each grid cell and month we identified the 75th percentile value across space (i.e. p_{75}) as threshold for extreme AOD for WRF-Chem and MODIS separately. Grid cells with AOD exceeding that threshold were classified as exhibiting extreme values. The consistency in the spatial distribution of extreme values as simulated by WRF-Chem relative to MODIS are quantified using three skill statistics: the Accuracy, Hit Rate (HR) and Threat Score (TS) defined in equations 5-74-6. In these equations, WE , ME , WN and MN correspond to ~~occurrence frequency~~ of extreme conditions in WRF-Chem (WE) or MODIS (ME) or not (WN or MN):

$$Accuracy = \frac{WE / ME + WN / MN}{WE / ME + WE / MN + WN / ME + WN / MN} \quad (54)$$

$$HR = \frac{WE / ME}{WE / ME + WN / ME} \quad (65)$$

$$TS = \frac{WE / ME}{WE / ME + WE / MN + WN / ME} \quad (76)$$

The Accuracy describes the fraction of grid cells co-identified as exceeding $p75$ or not in MODIS and WRF-Chem, and thus equally weights event and non-event conditions. Since the Accuracy quantifies model skill in correctly identifying both extreme and non-extreme aerosol loadings, it is thus indicative of model performance in capturing the overall AOD spatial variability. In this application, where extreme is identified as the 75th percentile, a value of 0.5 would indicate none of the grid cells experiencing extreme events were reproduced by the model, while 1 would indicate perfect identification of events and non-events. The HR and TS metrics give ‘credit’ only those grid cells identified as ‘extreme’. For these metrics, a value of 0 indicates no correct identification of grid cells with extreme values, while a perfect model would exhibit a value of 1.

2. Evaluation of the scales of coherence of extreme AOD. For each day during the overpass time and hours of clear sky conditions, we determine if AOD simulated at our reference location (i.e. the center of the domain, in Southern Indiana) is equal or larger than the local $p75$ for that grid cell and season and then identify all grid cells in the domain that also satisfy the condition of $AOD \geq \text{local } p75$. The reference location represents the center of gravity of the domain and was previously used by Sullivan et al. (2015) for assessing scales of coherence. In that work they also found the spatial scales of coherence are not sensitive to the precise choice of reference location. For each season, we thus compute the probability of extreme AOD co-occurrence at our reference site and any other grid cell as the frequency of co-occurrence divided by the number of extreme occurrences at the reference location. The spatial scales of extreme AOD are then estimated by binning the radial distance of each grid cell centroid from the domain center into 100 km distance classes. An analogous procedure is applied to L2 MODIS data to compare with simulations.

3. Results

3.1 Evaluation of AOD

Overall WRF-Chem is positively biased relative to remotely-sensed AOD. The spatial MFB is 0.1520 (0.14) when computed using all available MODIS measurements from Terra (Aqua)

and 0.50 relative to data from the AERONET stations (Table 3). The sign of this bias is consistent across the entire simulation domain (Fig. 2). These results agree with findings from previous regional studies that have also shown an overestimation of AOD by WRF-Chem over eastern North America and Europe (i.e. regions dominated by sulfate aerosols), and underestimation in western US and most of the rest of the globe (Zhang et al., 2012; Colarco et al., 2010; Curci et al., 2014) (Table 1). Higher biases of WRF-Chem simulated annual mean AOD are found in the southern portion of the domain (Fig. 2) where the model also exhibits a positive bias in daily mean near-surface $PM_{2.5}$ relative to observations from 1230 US EPA sites (see Fig. 3 and SM-Fig. S2). We further investigated the bias in $PM_{2.5}$ by comparing WRF-Chem simulations with ground-based measurements of particle composition at 123 IMPROVE sites over our domain. We computed the MFB on a seasonal basis between sulfate and nitrate concentrations in fine mode particles (i.e. Aitken and accumulation mode) versus observations (Fig. 4) and found sulfate concentrations are underestimated almost over the entire domain during winter, whereas a positive bias is present in the other seasons. Conversely, nitrates tend to be overestimated during winter and fall at most sites, whereas they are underestimated during summer. Thus the positive bias in AOD and $PM_{2.5}$ mass particularly during the summer appears to be associated with excess sulfate concentrations.

The MFB of WRF-Chem relative to MODIS estimates of AOD is lower than the MFB relative to most of the AERONET stations except for a few sites located along the coast, one polluted site in the northeast and a few land sites in the North/North-West (Fig. 2e-1 and 45a). This is possibly a result of an inability of the model to capture variations in aerosol optical properties occurring at a local scale (below the resolution of 12 km). However, the evaluation statistics for WRF-Chem relative to AERONET did not vary consistently with the classification of AERONET stations. Indeed, the mean MFB for AOD in coastal, polluted and land sites varies between 0.26 (coastal) and 0.67 (land), whereas for AE it varies between -0.72 (coastal) and -0.50 (land). When MODIS is compared to the 22 AERONET stations the MFB is -1.23 suggesting an underestimation of AOD from AERONET relative to MODIS. The large bias can be explained noting that the number of co-samples between MODIS is quite small and that MFB is strongly impacted by a few outliers. When we remove the three most biased sites (one land site in the North and two sites along the East coast) the MFB decreases to -0.91. Using very limited data, prior research indicated mesoscale variability (horizontal scales of 40–400 km and temporal scales of 2–48 h) is a common and perhaps universal feature of lower-tropospheric aerosol light extinction [Anderson et al., 2003]. However, we are not aware of

prior systematic attempts to quantify and test the universality of AOD scales of coherence over the contiguous US. To test the sensitivity of the MFB in simulated AOD to spatial aggregation, we excluded the first 12 cells to the left and to the top of the simulated domain and averaged the remaining 12×12 km grid cells over the following scales: 24×24, 36×36, 48×48, 72×72, 96×96, 144×144, 192×192, 216×216, 288×288, 384×384, 432×432, 576×576, 864×864, 1152×1152, 1728×1728, 3456×3456 km. The last spatial average corresponds to a single grid cell encompassing the entire domain (excluding the outer 12 cells located to the West and North of the simulation domain). Each spatial average at a coarser resolution is computed as the mean of all valid 12×12 km grid cells within the averaging area. We then computed the MFB for the regridded WRF-Chem and MODIS data pair and found that, on a yearly basis, MFB is highest at 12km (0.14 for Aqua and 0.15 for Terra) and reaches a first minimum at 72 km for Aqua (MFB=0.13) and 384 km for Terra (MFB=0.13) (see Fig. 6). However, the MFB and hence systematic error in AOD relative to MODIS exhibits only a weak dependence on the level of spatial aggregation.

Spatial patterns of monthly mean AOD show largest differences relative to MODIS during winter months in the southern states and near the coastlines, which show MFB up to 0.7, and lower spatial correlation (see Fig. 5a7a). This may be due to the larger uncertainty in MODIS retrievals near the coast (Anderson et al., 2013), the smaller sample size in the observations (particularly at high latitudes) during December to March or the lower overall AOD. Conversely, the spatial correlation is maximized ~~over~~-during the summer (r=0.5-0.7) for MODIS and August for MISR, when most data are available. The spatial variability of monthly mean AOD fields is also well simulated by WRF-Chem during the warm season (months May-August), as indicated by the ratio of the spatial standard deviation which is close to 1. However, $\sigma(\text{AOD})$ ~~it~~ is usually higher in MODIS and/or MISR than in WRF-Chem. The RMSD is largest and the spatial correlation is lowest during September and October, when MFB is also > 0.4 in part because WRF-Chem simulates high AOD and aerosol nitrate and sulfate concentrations over large regions in eastern North America (Fig. S3 and Fig. 4). The high positive bias in these months is also reflected in the near-surface PM_{2.5} concentrations and its composition (SM-Fig. S2 and Fig. 4). A possible explanation for the relatively poor model performance during September and October may derive from the simulation of precipitation. During the majority of calendar months, domain averaged precipitation as simulated by WRF-Chem is slightly positively biased relative to the gridded observational data. However, during September and October, the model exhibits a negative bias (of 8-10% relative to observations) and substantial

underestimation of precipitation in regions of typically high AOD such as the Ohio River valley and along the east coast (SM-FFig. 3S4). We also examined the impact of spatial aggregation (at 12, 24, 36, 48, 72 and 96 km resolution) on the seasonality of model performance. For AOD the spatial correlations are largest for most months when data are aggregated to a resolution of 24×24 km and the ratio of spatial standard deviation is also closer to 1 when AOD are spatially aggregated, possibly indicating that the spatial patterns simulated by WRF-Chem at a fine scale do not always match those observed by MODIS (Fig. 8). For AE both spatial correlations and ratio of standard deviations do not vary significantly when data are aggregated to a coarser resolution (Fig. S5).

Empirical quantile-quantile plots of AOD at AERONET stations computed for both simultaneous MODIS observations and WRF-Chem with AERONET observations indicate that the positive bias in WRF-Chem simulated values of AOD is evident across much of the probability distribution (5th to 95th percentile values) at most AERONET stations. However, it is worthy of note that WRF-Chem comparisons with AERONET observations occupy much of the same observational range as simultaneous MODIS and AERONET at those sites (Fig. 9a), although the EQQ plot does not necessarily compare the same MODIS-AERONET and WRF-Chem-AERONET data pairs (i.e. the sample used to compare AERONET and MODIS may differ from that used to compare WRF-Chem and AERONET due to the cloud screening procedure)same parameter space as simultaneous MODIS and AERONET observations at those sites (Fig. 6a). Thus, model simulations reproduce the range and probability of low-uncertainty AERONET measured AOD nearly as well as MODIS.

3.2 Evaluation of AE

Despite the low confidence in AE retrievals from MODIS, the comparison of WRF-Chem with the remote sensing estimates indicates some degree of agreement. The overall MFB of WRF-Chem vs MODIS Terra is -0.09 (-0.11 vs. Aqua) and the correlation between WRF-Chem and MODIS monthly mean AE seems to be independent of season and lies between 0.20 and 0.54 for all months except April, May and November when it is lower, whereas r is always < 0.14 when comparing with MISR (Fig. 7b).As described above, AE is retrieved with much lower confidence than AOD from the MODIS measurements. Nevertheless, the correlation between WRF-Chem and MODIS monthly mean AE seems to be independent of season and lies between 0.28 and 0.52 for all months except April, May and November when it is lower, whereas r is always < 0.25 when comparing with MISR (Fig. 5b). As for AOD, we computed the

~~Spearman's rank correlation coefficient to reduce the possible bias due to few outliers and the smaller sample size in MISR data (N varies between 2300–5500 depending on the month and is approximately 5 times smaller than the sample size for MODIS).~~ The AE RMSD relative to MODIS or MISR does not exhibit a clear seasonal pattern and the ratio of spatial standard deviations in the AE fields is always lower than 1, indicating more spatial variability in the satellite retrievals than in WRF-Chem. The degree to which these results are symptomatic of the difficulties in retrieving AE from the remote sensing observations is unclear. When the AE values are treated as binary samples ($\text{AE} < 1$ indicating coarse mode aerosols dominate, while $\text{AE} > 1$ indicating a dominance of the fine mode) and presented as a contingency table, WRF-Chem and MODIS simultaneously identify coarse mode dominance (i.e. $\text{AE} < 1$) in 18% of grid cells (Table 5). ~~After cloud screening,~~ WRF-Chem simulates 31% of grid cells as exhibiting annual mean $\text{AE} > 1$, while MODIS indicates a larger fraction of grid cells with $\text{AE} > 1$ (80%, Table 5). Both WRF-Chem and MODIS indicate the highest prevalence of fine mode particles during the warm months with highest agreement for co-identification (above 50%) during June-September. Co-identification of coarse mode particles is highest in the winter and spring months (above 20% during February-May and December, Table 5). However, when a χ^2 test is applied to the frequency of fine and coarse particles identified by WRF-Chem and MODIS, for all months except January and April, the p-value is < 0.01 , thus we reject the null hypothesis of equal distribution of fine and coarse mode particles identified by MODIS and WRF-Chem. The two data sets agree on 29% of the cases when trying to identify fine mode particles and approximately 53% of the cells are misclassified with MODIS usually identifying a high prevalence of fine aerosols than WRF-Chem. AE from WRF-Chem is also negatively biased relative to AERONET observations, with MFB = -0.59 indicating ~~WRF-Chem is simulating~~ a greater prevalence of coarse mode aerosols in the simulations (Table 3, Fig. 2 ~~and Fig. 4b~~).

EQQ plots for all sites show good accord between WRF-Chem and AERONET observations, as indicated by the relatively consistent fractional error across the entire range of simulated and observed AE (Fig. ~~6b~~9b). Simulations from previous studies have also shown a systematic negative bias of simulated AE versus MODIS observations. AE is very difficult to derive from the MODIS measurements and the uncertainty in AE scales with AOD (AE is very uncertain at $\text{AOD} < 0.2$). Further, AE is derived from wavelength dependent AOD, thus the uncertainties on the measurements are certainly correlated. As indicated in Figure 5, for some AERONET sites there is evidence that positive bias in AOD is associated with high negative bias in AE,

but this does not uniformly occur over eastern North America (e.g. for the site at 77.8W 55.3N WRF-Chem exhibits positive bias in AOD across the entire pdf while the simulated AE is negative biased, but the site at 84.28W 35.95N exhibits relative good accord for AOD but is negative biased in AE almost to the same amount as the northern station). -Highest biases have been noted in regions dominated by dust aerosols or when the model overestimates the dust loading, since aerosol population mean diameter is inversely proportional to AE (Colarco et al., 2014; Balzarini et al., 2014). Sources of the biases in our study, include the simplified treatment of the size distribution, weaknesses in the emission inventory or uncertainties in meteorological variables affecting particle growth (e.g. temperature and relative humidity). Future work will focus on examining these sensitivities.

3.3 AOD Extremes

Averaged across the entire simulation period, WRF-Chem correctly identifies 70% of locations with extreme and non-extreme AOD in the MODIS observations (i.e. the Accuracy = 70%, Table 6). The overall *TS* and *HR* also indicate the geographic location of extreme AOD is similar between the model and satellite retrievals. The annual mean *HR*, which is defined as the proportion of grid cells with extreme AOD co-identified by WRF-Chem and MODIS relative to MODIS extremes, is 41%. The annual mean *TS*, which also takes into account false alarms, is 27% (Table 6).

For each month, the *HR* is significantly higher than the probability of co-identification of

extremes by random chance (i.e. $p_0 = 0.25^2 = 0.0625$), since the test statistic $\frac{HR - p_0^2}{\sqrt{\frac{p_0 \times (1 - p_0)}{N}}}$ is

always larger than the critical value at 1% (i.e. 2.575). *HR* and *TS* vary seasonally, with highest skill during summer months (*HR* up to 70% and *TS* up to 54%), and lowest skill during winter and early spring (minimum *HR*=29% and minimum *TS*=17%) (Table 6 and Fig. 710). The relatively low skill in identifying the spatial occurrence of high AOD during winter and spring may reflect the relatively low AOD and low spatial variability during this season, which means ‘extreme’ AOD may differ only marginally from the ‘non-extreme’ areas (see SM-Fig. 4S6 for monthly comparisons of extreme area identification).

The spatial distribution of extreme AOD also displays some seasonality with areas of AOD > p_{75} concentrated over coastal regions and the southern states during summer months and

smaller areas during winter and early spring (Fig. 710). Despite the relatively low simultaneous
 identification of extremes during cold seasons, the location of extremes moves from the coast
 to the Great Lakes region and Midwest states in both the model and MODIS (see SM-Fig. 3S6).
 During winter and spring months WRF-Chem simulates more areas with extreme AOD over
 coastal regions, whereas MODIS shows more spatial variability and predicts higher AOD in
 the Great Lakes area and in the states west of Illinois. Conversely, WRF-Chem underestimates
 areas of extreme AOD relative to MODIS in the northern regions of the domain, possibly due
 to the underestimation of sulfate-aerosol. These two observations may be explained by noting
 that the mass fraction of aerosol nitrate in the accumulation and coarse mode predicted by WRF-
 Chem during most of fall and winter months dominates the sulfate fraction over virtually all of
 the domain (see SM-Fig. 5S3), whereas point observations indicate aerosol nitrate mass fraction
 is dominant only over the Central Great Plains (Hand et al., 2012). This may be related to an
 overestimation of aerosol-nitrate in winter and fall (Fig. 4) as a result of the impact of air
 temperature and relative humidity on aerosol ammonium nitrate (NH_4NO_3) stability
 (Aksoyoglu et al., 2011), as well as an underestimation of aerosol sulfate, mostly during winter
 (Fig. 4), likely due to underestimation of the rate of SO_2 gaseous and aqueous (missing)
 oxidation, or underestimation of the nighttime boundary layer height which impacts sulfate
 formation near the surface (Tuccella et al., 2012). Localized negative biases in the model over
 the coast may be associated with the higher uncertainties in MODIS retrievals at coastlines
 (Anderson et al., 2013).

Extreme AOD exhibits relatively large spatial scales of coherence in both the WRF-Chem
 simulations and MODIS L2 observations (Fig. 811). Consistent with prior analyses of L3
 MODIS data (Sullivan et al., 2015), the largest scales of coherence are found in fall. In all
 seasons except for winter the probability of co-occurrence of extremes at the domain center and
 any other grid cell in the simulation domain is > 0.5 up to a distance of 300 km. The simulated
 mean seasonal scales of extreme coherence are comparable to L2 MODIS AOD (Fig. 811),
 despite the larger variability in the MODIS data due to the limited retrievals with simultaneous
 extreme AOD at the reference location and each other grid cell. Thus, consistent with prior
 research this analysis indicates the occurrence of extreme AOD occurs on large spatial scales
 and therefore may significantly impact regional climate.

4. Discussion and concluding remarks

Aerosol direct and indirect radiative forcing on the climate system are highly uncertain. A systematic assessment of the ability of global and regional models to reproduce aerosol optical properties in the contemporary climate is essential to increasing confidence in future projections. We contribute to this growing literature by presenting high resolution (12 km) simulations from WRF-Chem conducted over eastern North America during a year representative of average meteorological and aerosol conditions. We evaluate the simulations relative to, and compare the results with daily MODIS and MISR observations, highas well as with high frequency AERONET measurements of AOD and AE and near-surface PM_{2.5} mass and composition measurements. -Results from this study show:

- After grid cells with any cloud presence are removed and considering only overpass hours, the domain averaged simulated mean AOD is 0.22. Simulated AOD is positively biased relative to observations, with MFB=0.14 when comparing with MODIS-Aqua and 0.39-50 relative to AERONET (Fig. 2-1 and 42). A clear north-south gradient in AOD bias vs. MODIS is also observed. This positive bias is consistent across the entire probability distribution at most AERONET stations (Fig. 69), and is also evident in comparison of modeled near-surface PM_{2.5} mass relative to daily mean observations distributed at 1230 stations across the domain (Fig. 3).
- Model skill in reproducing the spatial fields of monthly mean AOD as measured by the spatial correlation and ratio of the spatial variability with MODIS is maximized during the summer months ($r \sim 0.5-0.7$, and ratio of $\sigma \sim 0.8$ to 1.2). During this season observed AOD is higher and more observations are available (Fig. 57). Lowest model-observations agreement is found in September and October and is at least partially attributable to a dry bias in precipitation from WRF-Chem (~~SM~~Fig. 3S4).
- In part because of the difficulties in retrieving robust estimates of AE, few previous studies have evaluated model simulated AE values. We show that AE as simulated by WRF-Chem over eastern North America is negatively biased relative to MODIS (MFB=-0.10) and AERONET (MFB=-0.6459). This bias indicates WRF-Chem simulates a larger fraction of coarse mode particles than is evident in the remote sensing observations (see Table 3 and 5). While some of the bias relative to MODIS may reflect high observational uncertainty, the- large bias relative to AERONET is consistent with

prior research (Table 1), and is symptomatic of substantial systematic error in the aerosol size distribution.

- ~~the bias relative to AERONET is consistent with prior research (Table 1) and is symptomatic of relatively poor model performance for this metric.~~ Causes of the model error may include insufficiently detailed treatment of size distribution or inaccurate representation of aerosol composition and mixing state which affect the simulated size distribution and thus AE (Li et al., 2015; Curci et al., 2014)). Further, weaknesses in the emission inventory (e.g. size resolution of primary emissions), as suggested by the systematic bias in simulated PM_{2.5} concentrations relative to ground-based observations, and/or biases in the representation of meteorological conditions critical to determining aerosol nitrate concentrations may also affect model performance. Currently it is not possible to fully attribute the relative importance of these error sources.
- The majority of prior model evaluation exercises have tended to focus on mean AOD values~~the central tendency of the AOD probability distribution~~. However, the climate and health impacts of aerosols are ~~maximized-greater~~ under high aerosol loadings. We demonstrate that WRF-Chem exhibits some skill in capturing the spatial patterns of extreme aerosol loading, especially during summer months. During this season, the Hit Rate for AOD > p75 reaches 70%. Largest biases are found during winter months and near the coastlines where AOD from MODIS also exhibits largest retrieval uncertainty.

Despite the encouraging performance of WRF-Chem both in terms of simulation efficiency and in reproducing AOD (mean and extreme values) and the partial skill in reproducing AE over eastern North America, further investigations are needed to properly quantify the value added by running high-resolution simulations by direct comparison with analogous runs at coarser resolution. Future simulations will also involve assessment of accuracy of different aerosol schemes (i.e. sectional vs. modal approaches) to represent the size distribution. The inclusion of a direct description of new particle formation processes within WRF-Chem may also improve estimates of ultrafine particle concentrations and thus of simulated aerosol optical properties.

5. Acknowledgements

This research was supported in part by Lilly Endowment, Inc., through its support for the Indiana University Pervasive Technology Institute, and in part by the Indiana METACyt Initiative. The Indiana METACyt Initiative at IU is also supported in part by Lilly Endowment,

Inc. Additional support was provided by the L'Oréal-UNESCO UK and Ireland Fellowship For Women In Science (to PC), the Natural Environmental Research Council (NERC) through the LICS project (ref. NE/K010794/1), the US NSF (grants # 1102309 and 1517365 to SCP) and a NASA Earth and Space Science Fellowship Program - Grant "14-EARTH14F-0207" (to RCS). The data used in this study were acquired as part of the NASA's Earth-Sun System Division, and archived and distributed by the MODIS Level 1 and Atmosphere Archive and Distribution System (LAADS), and the Giovanni online data system, developed and maintained by the NASA Goddard Earth Sciences (GES) Data and Information Services Center (DISC). We thank the PI investigators and their staff for establishing and maintaining the 22 AERONET sites used in this investigation. PM_{2.5} surface concentrations from the United States Environmental Protection Agency were obtained from: http://www.epa.gov/airquality/airdata/ad_data_daily.html. Meteorological lateral boundary conditions from the North American Mesoscale model were obtained from the NOAA Operational Model Archive and Distribution System: ftp://nomads.ncdc.noaa.gov/NAM/analysis_only/.

6. References

- Ackermann, I. J., Hass, H., Memmesheimer, M., Ebel, A., Binkowski, F. S., and Shankar, U.: Modal aerosol dynamics model for Europe: development and first applications, *Atmos. Environ.*, 32, 2981-2999, [http://dx.doi.org/10.1016/S1352-2310\(98\)00006-5](http://dx.doi.org/10.1016/S1352-2310(98)00006-5), 1998.
- Aksoyoglu, S., Keller, J., Barmpadimos, I., Oderbolz, D., Lanz, V. A., Prévôt, A. S. H., and Baltensperger, U.: Aerosol modelling in Europe with a focus on Switzerland during summer and winter episodes, *Atmos. Chem. Phys.*, 11, 7355-7373, 10.5194/acp-11-7355-2011, 2011.
- Alston, E. J., Sokolik, I. N., and Kalashnikova, O. V.: Characterization of atmospheric aerosol in the US Southeast from ground- and space-based measurements over the past decade, *Atmospheric Measurement Techniques*, 5, 1667-1682, 10.5194/amt-5-1667-2012, 2012.
- Anderson, J. C., Wang, J., Zeng, J., Leptoukh, G., Petrenko, M., Ichoku, C., and Hu, C.: Long-term statistical assessment of Aqua-MODIS aerosol optical depth over coastal regions: bias characteristics and uncertainty sources, *Tellus Series B-Chemical and Physical Meteorology*, 65, 10.3402/tellusb.v65i0.20805, 2013.
- Anderson, J. R., Hardy, E. E., Roach, J. T., and Witmer, R. E.: A land use and land cover classification system for use with remote sensor data, Report 964, 1976.
- Anderson, T. L., Charlson, R. J., Winker, D. M., Ogren, J. A., and Holmén, K.: Mesoscale Variations of Tropospheric Aerosols*, *Journal of the Atmospheric Sciences*, 60, 119-136, 10.1175/1520-0469(2003)060<0119:MVOTA>2.0.CO;2, 2003.
- Balzarini, A., Pirovano, G., Honzak, L., Žabkar, R., Curci, G., Forkel, R., Hirtl, M., San José, R., Tuccella, P., and Grell, G. A.: WRF-Chem model sensitivity to chemical mechanisms choice

688 in reconstructing aerosol optical properties, *Atmos. Environ.*,
689 <http://dx.doi.org/10.1016/j.atmosenv.2014.12.033>, 2014.

690 Boucher, O., D. Randall, and P. Artaxo, C. B., G. Feingold, P. Forster, V.-M. Kerminen, Y.
691 Kondo, H. Liao, U. Lohmann, P. Rasch, S.K. Satheesh, S. Sherwood, B. Stevens and X.Y.
692 Zhang: Clouds and Aerosols, in: *Climate Change 2013: The Physical Science Basis*.
693 Contribution of Working Group I to the Fifth Assessment Report of the Intergovernmental
694 Panel on Climate Change, edited by: Stocker, T. F., D. Qin, G.-K. Plattner, M. Tignor, S.K.
695 Allen, J. Boschung, A. Nauels, Y. Xia, V. Bex and P.M. Midgley, Cambridge University Press,
696 Cambridge, United Kingdom and New York, NY, USA, 33–115, 2013.

697 Boylan, J. W., and Russell, A. G.: PM and light extinction model performance metrics, goals,
698 and criteria for three-dimensional air quality models, *Atmos. Environ.*, 40, 4946-4959,
699 <http://dx.doi.org/10.1016/j.atmosenv.2005.09.087>, 2006.

700 Castro, C. L., Pielke, R. A., and Leoncini, G.: Dynamical downscaling: Assessment of value
701 retained and added using the Regional Atmospheric Modeling System (RAMS), *Journal of*
702 *Geophysical Research: Atmospheres*, 110, D05108, 10.1029/2004JD004721, 2005.

703 Chu, S. H.: PM_{2.5} episodes as observed in the speciation trends network, *Atmos. Environ.*, 38,
704 5237-5246, 10.1016/j.atmosenv.2004.01.055, 2004.

705 Colarco, P., da Silva, A., Chin, M., and Diehl, T.: Online simulations of global aerosol
706 distributions in the NASA GEOS-4 model and comparisons to satellite and ground-based
707 aerosol optical depth, *J. Geophys. Res.-Atmos.*, 115, 10.1029/2009jd012820, 2010.

708 Colarco, P., Kahn, R. A., Remer, L. A., and Levy, R. C.: Impact of satellite viewing-swath
709 width on global and regional aerosol optical thickness statistics and trends, *Atmospheric*
710 *Measurement Techniques*, 7, 2313-2335, 10.5194/amt-7-2313-2014, 2014.

711

712 Curci, G., Hogrefe, C., Bianconi, R., Im, U., Balzarini, A., Baró, R., Brunner, D., Forkel, R.,
713 Giordano, L., Hirtl, M., Honzak, L., Jiménez-Guerrero, P., Knote, C., Langer, M., Makar, P.
714 A., Pirovano, G., Pérez, J. L., San José, R., Syrakov, D., Tuccella, P., Werhahn, J., Wolke, R.,
715 Žabkar, R., Zhang, J., and Galmarini, S.: Uncertainties of simulated aerosol optical properties
716 induced by assumptions on aerosol physical and chemical properties: An AQMEII-2
717 perspective, *Atmos. Environ.*, <http://dx.doi.org/10.1016/j.atmosenv.2014.09.009>, 2014.

718 de Meij, A., Pozzer, A., Pringle, K. J., Tost, H., and Lelieveld, J.: EMAC model evaluation and
719 analysis of atmospheric aerosol properties and distribution with a focus on the Mediterranean
720 region, *Atmospheric Research*, 114–115, 38-69,
721 <http://dx.doi.org/10.1016/j.atmosres.2012.05.014>, 2012.

722 Drury, E., Jacob, D. J., Spurr, R. J. D., Wang, J., Shinozuka, Y., Anderson, B. E., Clarke, A.
723 D., Dibb, J., McNaughton, C., and Weber, R.: Synthesis of satellite (MODIS), aircraft
724 (ICARTT), and surface (IMPROVE, EPA-AQS, AERONET) aerosol observations over eastern
725 North America to improve MODIS aerosol retrievals and constrain surface aerosol
726 concentrations and sources, *J. Geophys. Res.-Atmos.*, 115, 10.1029/2009jd012629, 2010.

727 Emmons, L. K., Walters, S., Hess, P. G., Lamarque, J. F., Pfister, G. G., Fillmore, D., Granier,
728 C., Guenther, A., Kinnison, D., Laepple, T., Orlando, J., Tie, X., Tyndall, G., Wiedinmyer, C.,
729 Baughcum, S. L., and Kloster, S.: Description and evaluation of the Model for Ozone and
730 Related chemical Tracers, version 4 (MOZART-4), *Geoscientific Model Development*, 3, 43-
731 67, 2010.

- Fast, J. D., Gustafson, W. I., Easter, R. C., Zaveri, R. A., Barnard, J. C., Chapman, E. G., Grell, G. A., and Peckham, S. E.: Evolution of ozone, particulates, and aerosol direct radiative forcing in the vicinity of Houston using a fully coupled meteorology-chemistry-aerosol model, *Journal of Geophysical Research: Atmospheres*, 111, D21305, 10.1029/2005JD006721, 2006.
- Ford, B., and Heald, C. L.: Aerosol loading in the Southeastern United States: reconciling surface and satellite observations, *Atmospheric Chemistry and Physics*, 13, 9269-9283, 10.5194/acp-13-9269-2013, 2013.
- Giannouli, M., Kalognomou, E.-A., Mellios, G., Moussiopoulos, N., Samaras, Z., and Fiala, J.: Impact of European emission control strategies on urban and local air quality, *Atmos. Environ.*, 45, 4753-4762, 10.1016/j.atmosenv.2010.03.016, 2011.
- Gkikas, A., Houssos, E. E., Hatzianastassiou, N., Papadimas, C. D., and Bartzokas, A.: Synoptic conditions favouring the occurrence of aerosol episodes over the broader Mediterranean basin, *Quarterly Journal of the Royal Meteorological Society*, 138, 932-949, 10.1002/qj.978, 2012.
- Grell, G. A., Peckham, S. E., Schmitz, R., McKeen, S. A., Frost, G., Skamarock, W. C., and Eder, B.: Fully coupled "online" chemistry within the WRF model, *Atmos. Environ.*, 39, 6957-6975, 10.1016/j.atmosenv.2005.04.027, 2005.
- Guenther, A., Zimmerman, P., and Wildermuth, M.: Natural volatile organic compound emission rate estimates for U.S. woodland landscapes, *Atmos. Environ.*, 28, 1197-1210, 10.1016/1352-2310(94)90297-6, 1994.
- Guenther, A. B., Zimmerman, P. R., Harley, P. C., Monson, R. K., and Fall, R.: Isoprene and monoterpene emission rate variability: model evaluations and sensitivity analyses, *J. Geophys. Res.-Atmos.*, 98, 12609-12617, 10.1029/93jd00527, 1993.
- Kovacs, T. (2006). "Comparing MODIS and AERONET aerosol optical depth at varying separation distances to assess ground-based validation strategies for spaceborne lidar." *J. Geophys. Res.-Atmos.* 111(D24).
- Hand, J. L., Schichtel, B. A., Pitchford, M., Malm, W. C., and Frank, N. H.: Seasonal composition of remote and urban fine particulate matter in the United States, *Journal of Geophysical Research: Atmospheres*, 117, D05209, 10.1029/2011JD017122, 2012.
- Hyer, E. J., Reid, J. S., and Zhang, J.: An over-land aerosol optical depth data set for data assimilation by filtering, correction, and aggregation of MODIS Collection 5 optical depth retrievals, *Atmospheric Measurement Techniques*, 4, 379-408, 10.5194/amt-4-379-2011, 2011.
- Holben, B. N., Eck, T. F., Slutsker, I., Tanre, D., Buis, J. P., Setzer, A., Vermote, E., Reagan, J. A., Kaufman, Y. J., Nakajima, T., Lavenu, F., Jankowiak, I., and Smirnov, A.: AERONET - A federated instrument network and data archive for aerosol characterization, *Remote Sensing of Environment*, 66, 1-16, 10.1016/s0034-4257(98)00031-5, 1998.
- Holben, B. N., Tanre, D., Smirnov, A., Eck, T. F., Slutsker, I., Abuhassan, N., Newcomb, W. W., Schafer, J. S., Chatenet, B., Lavenu, F., Kaufman, Y. J., Castle, J. V., Setzer, A., Markham, B., Clark, D., Frouin, R., Halthore, R., Karneli, A., O'Neill, N. T., Pietras, C., Pinker, R. T., Voss, K., and Zibordi, G.: An emerging ground-based aerosol climatology: Aerosol optical depth from AERONET, *J. Geophys. Res.-Atmos.*, 106, 12067-12097, 10.1029/2001jd900014, 2001.

775 Kahn, R. A., Gaitley, B. J., Martonchik, J. V., Diner, D. J., Crean, K. A., and Holben, B.:
776 Multiangle Imaging Spectroradiometer (MISR) global aerosol optical depth validation based
777 on 2 years of coincident Aerosol Robotic Network (AERONET) observations, *J. Geophys.*
778 *Res.-Atmos.*, 110, 10.1029/2004jd004706, 2005.

779 Kahn, R. A., Gaitley, B. J., Garay, M. J., Diner, D. J., Eck, T. F., Smirnov, A., and Holben, B.
780 N.: Multiangle Imaging SpectroRadiometer global aerosol product assessment by comparison
781 with the Aerosol Robotic Network, *J. Geophys. Res.-Atmos.*, 115, 10.1029/2010jd014601,
782 2010.

783 Kinne, S., O'Donnel, D., Stier, P., Kloster, S., Zhang, K., Schmidt, H., Rast, S., Giorgetta, M.,
784 Eck, T. F., and Stevens, B.: MAC-v1: A new global aerosol climatology for climate studies,
785 *Journal of Advances in Modeling Earth Systems*, 5, 704-740, 10.1002/jame.20035, 2013.

786 Kulmala, M., Asmi, A., Lappalainen, H. K., Baltensperger, U., Brenguier, J. L., Facchini, M.
787 C., Hansson, H. C., Hov, O., O'Dowd, C. D., Poeschl, U., Wiedensohler, A., Boers, R., Boucher,
788 O., de Leeuw, G., van der Gon, H. A. C. D., Feichter, J., Krejci, R., Laj, P., Lihavainen, H.,
789 Lohmann, U., McFiggans, G., Mentel, T., Pilinis, C., Riipinen, I., Schulz, M., Stohl, A.,
790 Swietlicki, E., Vignati, E., Alves, C., Amann, M., Ammann, M., Arabas, S., Artaxo, P., Baars,
791 H., Beddows, D. C. S., Bergstrom, R., Beukes, J. P., Bilde, M., Burkhardt, J. F., Canonaco, F.,
792 Clegg, S. L., Coe, H., Crumeyrolle, S., D'Anna, B., Decesari, S., Gilardoni, S., Fischer, M.,
793 Fjaeraa, A. M., Fountoukis, C., George, C., Gomes, L., Halloran, P., Hamburger, T., Harrison,
794 R. M., Herrmann, H., Hoffmann, T., Hoose, C., Hu, M., Hyvarinen, A., Horrak, U., Iinuma, Y.,
795 Iversen, T., Josipovic, M., Kanakidou, M., Kiendler-Scharr, A., Kirkevag, A., Kiss, G.,
796 Klimont, Z., Kolmonen, P., Komppula, M., Kristjansson, J. E., Laakso, L., Laaksonen, A.,
797 Labonnote, L., Lanz, V. A., Lehtinen, K. E. J., Rizzo, L. V., Makkonen, R., Manninen, H. E.,
798 McMeeking, G., Merikanto, J., Minikin, A., Mirme, S., Morgan, W. T., Nemitz, E., O'Donnell,
799 D., Panwar, T. S., Pawlowska, H., Petzold, A., Pienaar, J. J., Pio, C., Plass-Duelmer, C., Prevot,
800 A. S. H., Pryor, S., Reddington, C. L., Roberts, G., Rosenfeld, D., Schwarz, J., Seland, O.,
801 Sellegri, K., Shen, X. J., Shiraiwa, M., Siebert, H., Sierau, B., Simpson, D., Sun, J. Y., Topping,
802 D., Tunved, P., Vaattovaara, P., Vakkari, V., Veefkind, J. P., Visschedijk, A., Vuollekoski, H.,
803 Vuolo, R., Wehner, B., Wildt, J., Woodward, S., Worsnop, D. R., van Zadelhoff, G. J., Zardini,
804 A. A., Zhang, K., van Zyl, P. G., Kerminen, V. M., Carslaw, K. S., and Pandis, S. N.: General
805 overview: European Integrated project on Aerosol Cloud Climate and Air Quality interactions
806 (EUCAARI) - integrating aerosol research from nano to global scales, *Atmospheric Chemistry*
807 *and Physics*, 11, 13061-13143, 10.5194/acp-11-13061-2011, 2011.

808 Kumar, R., Barth, M. C., Pfister, G. G., Naja, M., and Brasseur, G. P.: WRF-Chem simulations
809 of a typical pre-monsoon dust storm in northern India: influences on aerosol optical properties
810 and radiation budget, *Atmospheric Chemistry and Physics*, 14, 2431-2446, 10.5194/acp-14-
811 2431-2014, 2014.

812 Kurokawa, J., Ohara, T., Morikawa, T., Hanayama, S., Janssens-Maenhout, G., Fukui, T.,
813 Kawashima, K., and Akimoto, H.: Emissions of air pollutants and greenhouse gases over Asian
814 regions during 2000-2008: Regional Emission inventory in ASia (REAS) version 2,
815 *Atmospheric Chemistry and Physics*, 13, 11019-11058, 10.5194/acp-13-11019-2013, 2013.

816 Lee, Y. H., Adams, P. J., and Shindell, D. T.: Evaluation of the global aerosol microphysical
817 ModelE2-TOMAS model against satellite and ground-based observations, *Geosci. Model Dev.*,
818 8, 631-667, 10.5194/gmd-8-631-2015, 2015.

819 Levy, R. C., Remer, L. A., and Dubovik, O.: Global aerosol optical properties and application
820 to Moderate Resolution Imaging Spectroradiometer aerosol retrieval over land, *J. Geophys.*
821 *Res.-Atmos.*, 112, 15, 10.1029/2006jd007815, 2007.

822 Levy, R. C., Remer, L. A., Kleidman, R. G., Mattoo, S., Ichoku, C., Kahn, R., and Eck, T. F.:
823 Global evaluation of the Collection 5 MODIS dark-target aerosol products over land,
824 *Atmospheric Chemistry and Physics*, 10, 10399-10420, 10.5194/acp-10-10399-2010, 2010.

825 Li, S., Kahn, R., Chin, M., Garay, M. J., and Liu, Y.: Improving satellite-retrieved aerosol
826 microphysical properties using GOCART data, *Atmos. Meas. Tech.*, 8, 1157-1171,
827 10.5194/amt-8-1157-2015, 2015.

828 Matsuura, K., and Willmott, C. J.: Terrestrial precipitation: 1900–2008 gridded monthly time
829 series, 2009.

830 Michou, M., Nabat, P., and Saint-Martin, D.: Development and basic evaluation of a prognostic
831 aerosol scheme (v1) in the CNRM Climate Model CNRM-CM6, *Geosci. Model Dev.*, 8, 501-
832 531, 10.5194/gmd-8-501-2015, 2015.

833 Myhre, G., Samset, B. H., Schulz, M., Balkanski, Y., Bauer, S., Bernsten, T. K., Bian, H.,
834 Bellouin, N., Chin, M., Diehl, T., Easter, R. C., Feichter, J., Ghan, S. J., Hauglustaine, D.,
835 Iversen, T., Kinne, S., Kirkevåg, A., Lamarque, J. F., Lin, G., Liu, X., Lund, M. T., Luo, G.,
836 Ma, X., van Noije, T., Penner, J. E., Rasch, P. J., Ruiz, A., Seland, O., Skeie, R. B., Stier, P.,
837 Takemura, T., Tsigaridis, K., Wang, P., Wang, Z., Xu, L., Yu, H., Yu, F., Yoon, J. H., Zhang,
838 K., Zhang, H., and Zhou, C.: Radiative forcing of the direct aerosol effect from AeroCom Phase
839 II simulations, *Atmospheric Chemistry and Physics*, 13, 1853-1877, 10.5194/acp-13-1853-
840 2013, 2013.

841 Nabat, P., Somot, S., Mallet, M., Michou, M., Sevault, F., Driouech, F., Meloni, D., di Sarra,
842 A., Di Biagio, C., Formenti, P., Sicard, M., Léon, J. F., and Bouin, M. N.: Dust aerosol radiative
843 effects during summer 2012 simulated with a coupled regional aerosol–atmosphere–ocean
844 model over the Mediterranean, *Atmos. Chem. Phys.*, 15, 3303-3326, 10.5194/acp-15-3303-
845 2015, 2015.

846 Nair, V. S., Solmon, F., Giorgi, F., Mariotti, L., Babu, S. S., and Moorthy, K. K.: Simulation of
847 South Asian aerosols for regional climate studies, *Journal of Geophysical Research:*
848 *Atmospheres*, 117, n/a-n/a, 10.1029/2011JD016711, 2012.

849 Pereira, S. N., Wagner, F., and Silva, A. M.: Seven years of measurements of aerosol scattering
850 properties, near the surface, in the southwestern Iberia Peninsula, *Atmospheric Chemistry and*
851 *Physics*, 11, 17-29, 10.5194/acp-11-17-2011, 2011.

852 Pfister, G. G., Parrish, D. D., Worden, H., Emmons, L. K., Edwards, D. P., Wiedinmyer, C.,
853 Diskin, G. S., Huey, G., Oltmans, S. J., Thouret, V., Weinheimer, A., and Wisthaler, A.:
854 Characterizing summertime chemical boundary conditions for airmasses entering the US West
855 Coast, *Atmos. Chem. Phys.*, 11, 1769-1790, 10.5194/acp-11-1769-2011, 2011.

856 Rea, G., Turquety, S., Menut, L., Briant, R., Mailler, S., and Siour, G.: Source contributions to
857 2012 summertime aerosols in the Euro-Mediterranean region, *Atmos. Chem. Phys. Discuss.*,
858 15, 8191-8242, 10.5194/acpd-15-8191-2015, 2015.

859 Remer, L. A., Kaufman, Y. J., Tanre, D., Mattoo, S., Chu, D. A., Martins, J. V., Li, R. R.,
860 Ichoku, C., Levy, R. C., Kleidman, R. G., Eck, T. F., Vermote, E., and Holben, B. N.: The
861 MODIS aerosol algorithm, products, and validation, *Journal of the Atmospheric Sciences*, 62,
862 947-973, 10.1175/jas3385.1, 2005.

863 Schell, B., Ackermann, I. J., Hass, H., Binkowski, F. S., and Ebel, A.: Modeling the formation
864 of secondary organic aerosol within a comprehensive air quality model system, *J. Geophys.*
865 *Res.-Atmos.*, 106, 28275-28293, 10.1029/2001jd000384, 2001.

866 Shepard, D.: A two-dimensional interpolation function for irregularly-spaced data, *Proceedings*
867 *of the 1968 23rd ACM national conference*, 1968.

868 Sič, B., El Amraoui, L., Marécal, V., Josse, B., Arteta, J., Guth, J., Joly, M., and Hamer, P. D.:
869 Modelling of primary aerosols in the chemical transport model MOCAGE: development and
870 evaluation of aerosol physical parameterizations, *Geosci. Model Dev.*, 8, 381-408,
871 10.5194/gmd-8-381-2015, 2015.

872 Simpson, D., Guenther, A., Hewitt, C. N., and Steinbrecher, R.: Biogenic emissions in Europe.
873 1. estimates and uncertainties, *J. Geophys. Res.-Atmos.*, 100, 22875-22890,
874 10.1029/95jd02368, 1995.

875 Spracklen, D. V., Carslaw, K. S., Merikanto, J., Mann, G. W., Reddington, C. L., Pickering, S.,
876 Ogren, J. A., Andrews, E., Baltensperger, U., Weingartner, E., Boy, M., Kulmala, M., Laakso,
877 L., Lihavainen, H., Kivekäs, N., Komppula, M., Mihalopoulos, N., Kouvarakis, G., Jennings,
878 S. G., O'Dowd, C., Birmili, W., Wiedensohler, A., Weller, R., Gras, J., Laj, P., Sellegri, K.,
879 Bonn, B., Krejci, R., Laaksonen, A., Hamed, A., Minikin, A., Harrison, R. M., Talbot, R., and
880 Sun, J.: Explaining global surface aerosol number concentrations in terms of primary emissions
881 and particle formation, *Atmos. Chem. Phys.*, 10, 4775-4793, 10.5194/acp-10-4775-2010, 2010.

882 Stocker, T. F., Qin, D., and Plattner, G.-K., Alexander, L.V., Allen, S.K., Bindoff, N.L., Bréon,
883 F.-M., Church, J.A., Cubasch, U., Emori, S., Forster, P., Friedlingstein, P., Gillett, N., Gregory,
884 J.M., Hartmann, D.L., Jansen, E., Kirtman, B., Knutti, R., Krishna Kumar, K. and Lemke, P.
885 and Marotzke, J., Masson-Delmotte, V., Meehl, G.A., Mokhov, I.I., Piao, S., Ramaswamy,
886 V., Randall, D., Rhein, M., Rojas, M., Sabine, C., Shindell, D., Talley, L.D., Vaughan, D.G.,
887 Xie, S.-P.: Summary for Policymakers, in: *Climate Change 2013: The Physical Science Basis.*
888 *Contribution of Working Group I to the Fifth Assessment Report of the Intergovernmental*
889 *Panel on Climate Change*, Cambridge University Press, Cambridge, United Kingdom and New
890 York, NY, USA, 33–115, 2013.

891 [Santese, M., F. De Tomasi and M. R. Perrone \(2007\). "AERONET versus MODIS aerosol](#)
892 [parameters at different spatial resolutions over southeast Italy." *J. Geophys. Res.-Atmos.*](#)
893 [112\(D10\).](#)

894 [Schutgens, N. A. J., M. Nakata and T. Nakajima \(2013\). "Validation and empirical correction](#)
895 [of MODIS AOT and AE over ocean." *Atmos. Meas. Techn.* 6\(9\): 2455-2475.](#)

896 [Shinozuka, Y. and J. Redemann \(2011\). "Horizontal variability of aerosol optical depth](#)
897 [observed during the ARCTAS airborne experiment." *Atmos. Chem. Phys.* 11\(16\): 8489-8495.](#)

898 Stockwell, W. R., Middleton, P., Chang, J. S., and Tang, X.: The second generation regional
899 acid deposition model chemical mechanism for regional air quality modeling, *Journal of*
900 *Geophysical Research: Atmospheres*, 95, 16343-16367, 10.1029/JD095iD10p16343, 1990.

901 Sullivan, R. C., Levy, R. C., and Pryor, S. C.: Spatiotemporal coherence of mean and extreme
902 aerosol particle events over eastern North America as observed from satellite, *Atmos. Environ.*,
903 112, 126-135, <http://dx.doi.org/10.1016/j.atmosenv.2015.04.026>, 2015.

904 Taylor, K. E.: Summarizing multiple aspects of model performance in a single diagram, *J.*
905 *Geophys. Res.-Atmos.*, 106, 7183-7192, 10.1029/2000jd900719, 2001.

906 Tessum, C. W., Hill, J. D., and Marshall, J. D.: Twelve-month, 12 km resolution North
 907 American WRF-Chem v3.4 air quality simulation: performance evaluation, *Geosci. Model*
 908 *Dev. Discuss.*, 7, 8433-8476, 10.5194/gmdd-7-8433-2014, 2014.

909 Tuccella, P., Curci, G., Visconti, G., Bessagnet, B., Menut, L., and Park, R. J.: Modeling of gas
 910 and aerosol with WRF/Chem over Europe: Evaluation and sensitivity study, *Journal of*
 911 *Geophysical Research: Atmospheres*, 117, D03303, 10.1029/2011JD016302, 2012.

912 Tuccella, P., Curci, G., Grell, G. A., Visconti, G., Crumeyrolle, S., Schwarzenboeck, A., and
 913 Mensah, A. A.: A new chemistry option in WRF/Chem v. 3.4 for the simulation of direct and
 914 indirect aerosol effects using VBS: evaluation against IMPACT-EUCAARI data, *Geosci.*
 915 *Model Dev. Discuss.*, 8, 791-853, 10.5194/gmdd-8-791-2015, 2015.

916 US-EPA: 2005 National Emissions Inventory (NEI), US Environmental Protection Agency
 917 available at: ftp://aftp.fsl.noaa.gov/divisions/taq/emissions_data_2005/, 2009.

918 Valenzuela, A., Olmo, F. J., Lyamani, H., Granados-Munoz, M. J., Anton, M., Guerrero-
 919 Rascado, J. L., Quirantes, A., Toledano, C., Perez-Ramirez, D., and Alados-Arboledas, L.:
 920 Aerosol transport over the western Mediterranean basin: Evidence of the contribution of fine
 921 particles to desert dust plumes over Alboran Island, *J. Geophys. Res.-Atmos.*, 119, 14028-
 922 14044, 10.1002/2014jd022044, 2014.

923 Willmott, C. J., Rowe, C. M., and Philpot, W. D.: Small-Scale Climate Maps: A Sensitivity
 924 Analysis of Some Common Assumptions Associated with Grid-Point Interpolation and
 925 Contouring, *The American Cartographer*, 12, 5-16, 10.1559/152304085783914686, 1985.

926 Wu, S., Mickley, L. J., Kaplan, J. O., and Jacob, D. J.: Impacts of changes in land use and land
 927 cover on atmospheric chemistry and air quality over the 21st century, *Atmospheric Chemistry*
 928 *and Physics*, 12, 1597-1609, 10.5194/acp-12-1597-2012, 2012.

929 Xing, J., Mathur, R., Pleim, J., Hogrefe, C., Gan, C. M., Wong, D. C., Wei, C., Gilliam, R., and
 930 Pouliot, G.: Observations and modeling of air quality trends over 1990-2010 across the
 931 Northern Hemisphere: China, the United States and Europe, *Atmospheric Chemistry and*
 932 *Physics*, 15, 2723-2747, 10.5194/acp-15-2723-2015, 2015.

933 Zhang, Y., Chen, Y., Sarwar, G., and Schere, K.: Impact of gas-phase mechanisms on Weather
 934 Research Forecasting Model with Chemistry (WRF/Chem) predictions: Mechanism
 935 implementation and comparative evaluation, *J. Geophys. Res.-Atmos.*, 117,
 936 10.1029/2011jd015775, 2012.

937 **Tables**

938 Table 1. Synthesis of some recent prior studies comparing simulated aerosol optical properties from global or regional model simulations with
 939 remote sensing products. The first column summarizes the model used, the second the domain and the time period simulated and the third shows
 940 the model resolution and summarizes the description of the aerosol size distribution. Columns 4 to 9 summarize the evaluation statistics in terms
 941 of the overall correlation coefficient (R), bias (as described using the mean fractional error (MFE)) and root mean square error (RMSE) or mean
 942 absolute error (MAE) relative to satellite or AERONET observations as reported in the references shown in column 10.

Model	Domain, Time	Resolution, Aerosol Approach	R AOD vs. Satellite	bias AOD vs. Satellite	R AOD vs. AERONET	bias AOD vs. AERONET	R AE vs. AERONE T	RMSE, MAE AE vs. AERONET	Ref
TOMAS in GISS	Global, 2000-2003	2°x2.5°, Sectional: 15 bins from 3 nm-10 µm	0.63 (average of monthly from 2004-2006, MODIS), 0.73 average of monthly from 2004-2006, MISR)	MFE: -29% (average of monthly from 2004- 2006, MODIS), -34% (average of monthly from 2004-2006, MISR)	-0.7-0.99 (monthly, 28)	-77-72% (monthly, 28)	N/A	N/A	(Lee et al., 2015)
GOCART with GEOS DAS	CONUS, 2006-2009	1°x1.25°, not specified	N/A	N/A	0.5 (2 hr. average at MISR overpass, 32)	N/A	0.43 (2 hr. average at MISR overpass, 32)	N/A	(Li et al., 2015)

GEMS/MACC aerosol module in CNRM-GAME and CERFACS	Global, 1993-2012	1.4°, Sectional, 12 bins	N/A	Mean relative bias -41- (-52)% (monthly, MISR)	<0-0.9 (monthly, 166)	N/A	N/A	N/A	(Michou et al., 2015)
CNRM-RCSM5	Mediterr., Summer 2012	50 km, Sectional, 12 bins	0.64 (seasonal, MODIS), 0.77 (seasonal, MISR), 0.65 (seasonal SEVIRI)	N/A	0.7 (daily, 30)	RMSE~1.75 (daily, 30)	N/A	N/A	(Nabat et al., 2015)
CHIMERE chemical transport model with WRF meteorology	Europe, Mediterr. -10°-40°E, 30°-55°N, Summer 2012	50 km, Sectional: 5 bins 40 nm-40 µm	0.35-0.75 (hourly, MODIS)	RMSE: 0.04-0.1 (hourly, MODIS)	0.44-0.73 (hourly, 65)	RMSE: 0.8- 0.11 (hourly, 65)	N/A	N/A	(Rea et al., 2015)
MOCAGE	Global, 2007	2°x2°, Sectional: 6 bins per species	0.322 (daily MODIS)	normalized mean bias 0.098 (daily MODIS)	N/A	N/A	N/A	N/A	(Sič et al., 2015)
WRF-Chem	0°-10°E, 50°- 55°N; -10°-15°E, 46°-57°N; -15°-30°E,	nested 2 - 30 km, modal	N/A	0.38±0.12 and 0.42±0.10 domain average AOD from MODIS and model respectively	N/A	N/A	N/A	N/A	(Tuccella et al., 2015)

	36°-62°N, 14-30 May 2008								
GOCART in GEOS	Global, 2000-2006	1°x1.25°, dust (8 bins 0.1-10 µm), sea salt (5 bins 0.03-10 µm), carbonaceous/sulfate (modal)	0.747, 0.72 E.US (monthly, MODIS)	N/A	0.707 (monthly, 53)	rms: 0.133 (monthly, 53)	0.81 (monthly, 53)	rms: 0.285 (monthly, 53)	(Colarco et al., 2010)
EMAC	Global, Year 2006	1.1°x1.1°, modal	N/A	Negative (North America)	0.27-0.60 (North America)	RMSE=0.1-0.2	>0.5 (Europe)	N/A	(de Meij et al., 2012)
GEOS-Chem	N. America, 06 July - 14 Aug 2004	2°x2.5°, modal	N/A	N/A	0.87 (study period mean, 24)	N/A	N/A	N/A	(Drury et al., 2010)
WRF-Chem	Europe and N. Africa, Year 2010	23 km, Modal and sectional (4 bins: 0.04-10 µm)	N/A	N/A	0.52 (mod) 0.51 (sect)	NMB=- 0.06(mod) NMB=-0.21 (sect) (daily, 12 stations)	N/A	N/A	(Balzarini et al., 2014)
RegCM4	South Asia,	50 km,	N/A	N/A	0.47-0.71	N/A	N/A	N/A	(Nair et al., 2012)

	2005-2007	Sectional (4 bins: 0.01-20 μm)			Monthly, 6				
--	-----------	---	--	--	------------	--	--	--	--

943

944 Table 2. Physical and chemical schemes adopted in the WRF-Chem simulations presented
 945 herein.

Simulation settings	Values
Domain size	300 × 300 cells
Horizontal resolution	12 km
Vertical resolution	32 levels up to 50 hPa
Timestep for physics	72 s
Timestep for chemistry	5 s
Physics option	Adopted scheme
Microphysics	WRF Single-Moment 5-class
Longwave Radiation	Rapid Radiative Transfer Model (RRTM)
Shortwave Radiation	Goddard
Surface layer	Monin Obhukov similarity
Land Surface	Noah Land Surface Model
Planetary boundary layer	Mellor-Yamada-Janjich
Cumulus parameterizations	Grell 3
Chemistry option	Adopted scheme
Photolysis	Fast J
Gas-phase chemistry	RADM2
Aerosols	MADE/SORGAM
Anthropogenic emissions	NEI (2005)
Biogenic emissions	Guenther, from USGS land use classification

946

947

Table 3. Spatial Mean Fractional Bias (MFB) over the entire year. Recall

$$MFB = \frac{1}{N} \sum_1^N \frac{C_m - C_0}{\frac{C_m + C_0}{2}}, \text{ where } C_m \text{ is the monthly mean AOD or AE simulated by WRF-Chem}$$

at a specific location and C_0 refers to the same quantity from MODIS/MISR/AERONET. Thus a negative value indicates the model is negatively biased relative to the observations. The total sample size N is 358,048 and 359,633 when comparing WRF-Chem with MODIS onboard Terra and Aqua respectively. The comparison between MODIS and AERONET is affected by a few outlier sites, so in parenthesis is the MFB when the three most biased sites are removed. The mean domain averaged AOD and AE from WRF-Chem (after applying the cloud screen and selecting only MODIS overpass hours) are 0.222 and 1.089, respectively.

Comparisons	MFB AOD	MFB AE
WRF-MODIS (Terra)	0. 20 <u>15</u>	-0.09
WRF-MODIS (Aqua)	0.14	-0.11
WRF-MISR (Terra)	0.16	-0.11
WRF-AERONET	0.50	-0.59
MODIS (Terra)-AERONET	-1.23 <u>(-0.91)</u>	-0.13 <u>(-0.11)</u>

960 Table 4. Contingency table used to compare the fraction of grid cells classified as fine ($AE >$
 961 1) and coarse ($AE < 1$) by MODIS and WRF-Chem.

		MODIS	
		Fine	Coarse
WRF-Chem	Fine	WF/MF	WF/MC
	Coarse	WC/MF	WC/MC

962

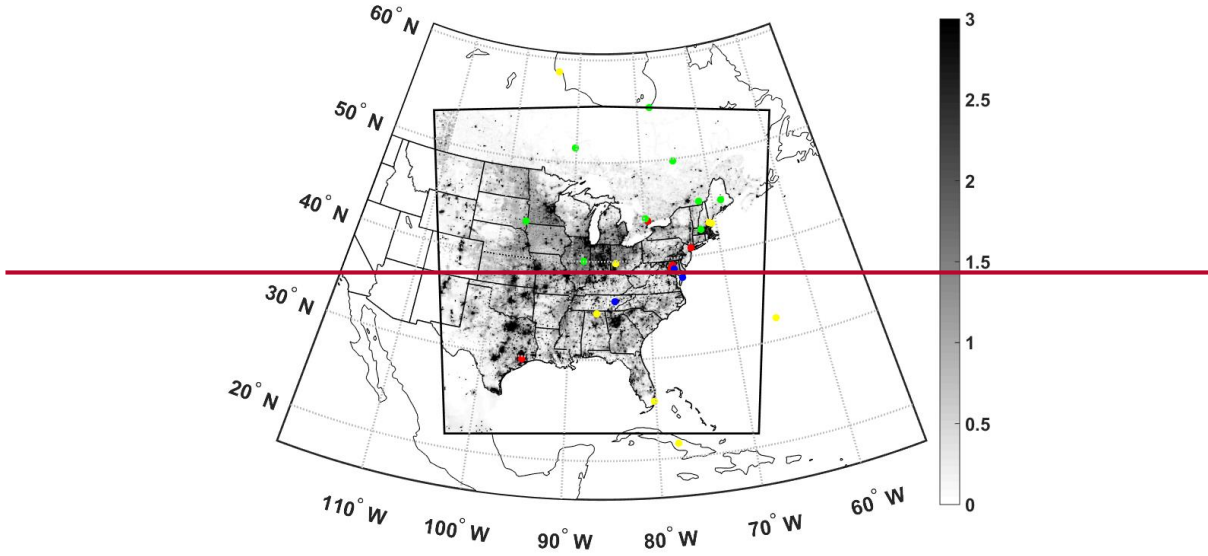
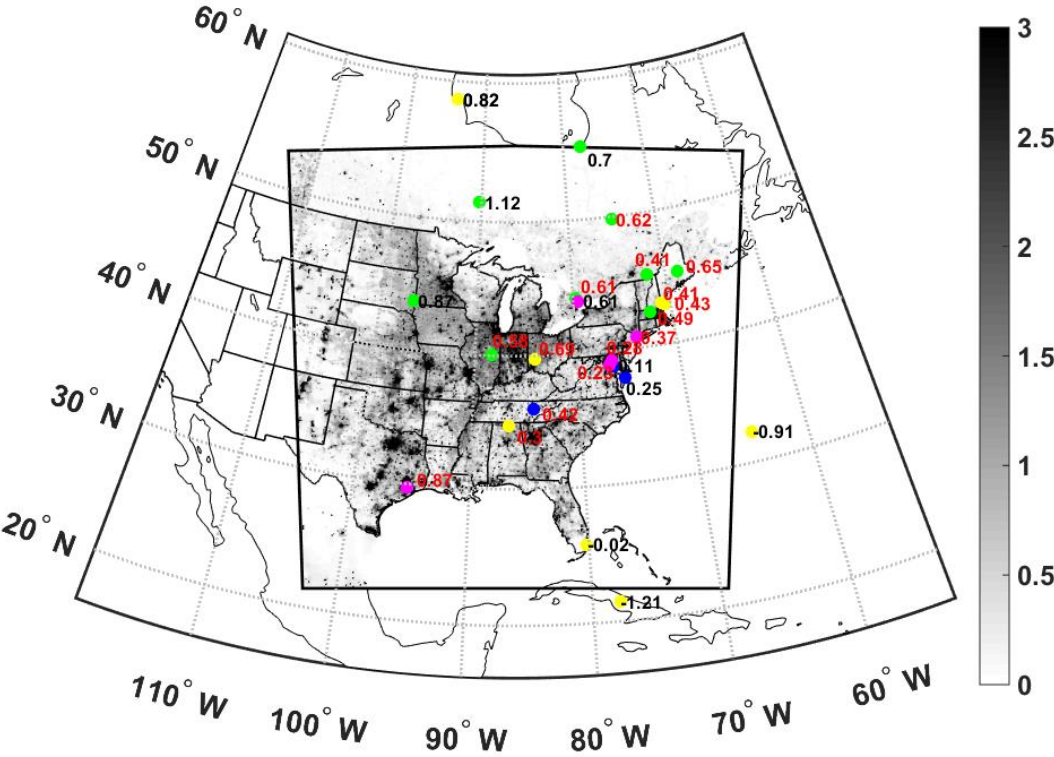
963

Table 5. Contingency table showing the fraction of grid cells simultaneously identified as fine (WF/MF) or coarse (WC/MC) mode particles by WRF-Chem and MODIS, as well as cells with different classification (columns 4 and 5). Recall a threshold of $AE = 1$ is used to define fine ($AE > 1$) and coarse mode ($AE < 1$) dominance. Months in bold indicate the distribution of observed and simulated fine/coarse mode fractions are significantly different (p-value < 0.01) according to the χ^2 test described in Sect. 2.3.

Month	WF/MF	WC/MC	WF/MC	WC/MF
1	0.025	0.176	0.007	0.792
2	0.030	0.241	0.004	0.725
3	0.005	0.297	0.001	0.697
4	0.013	0.230	0.004	0.753
5	0.141	0.204	0.028	0.628
6	0.541	0.122	0.055	0.283
7	0.623	0.094	0.030	0.252
8	0.520	0.061	0.017	0.402
9	0.561	0.118	0.032	0.288
10	0.486	0.145	0.088	0.281
11	0.321	0.179	0.058	0.442
12	0.164	0.248	0.015	0.573
mean	0.286	0.176	0.028	0.510

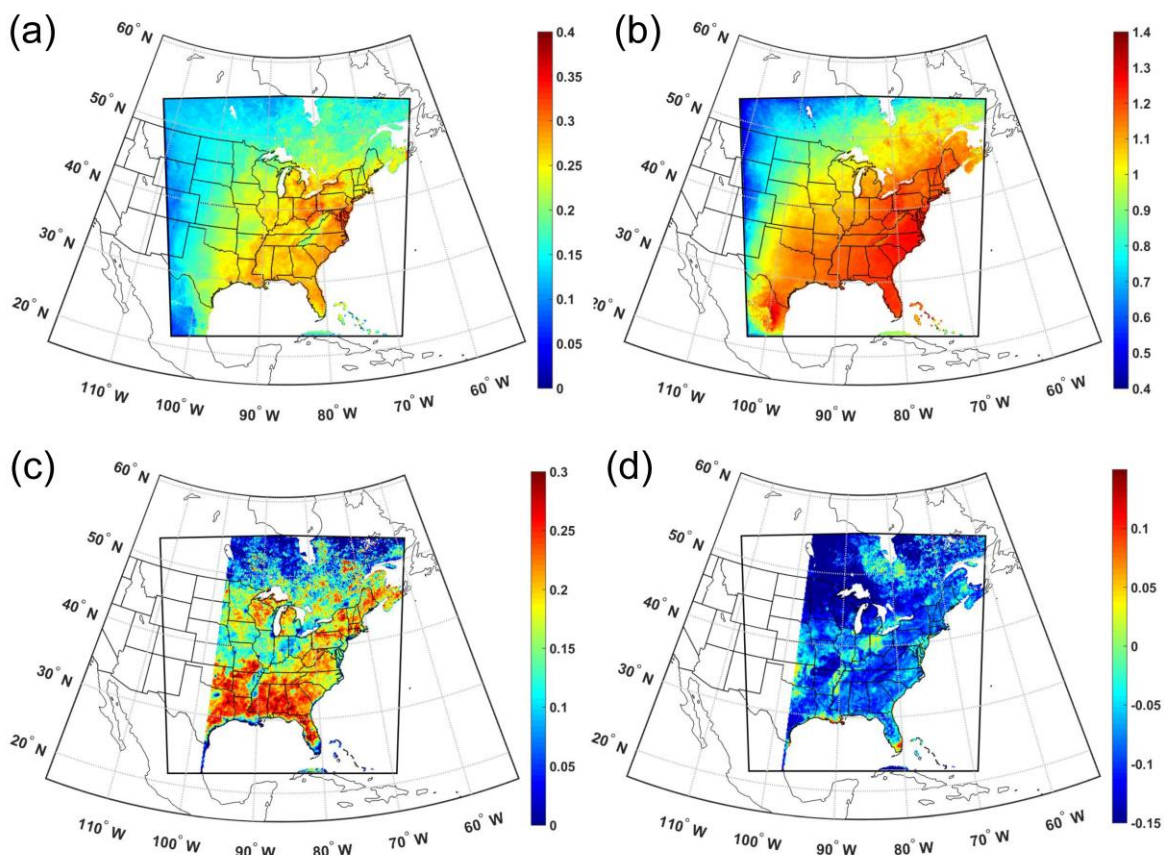
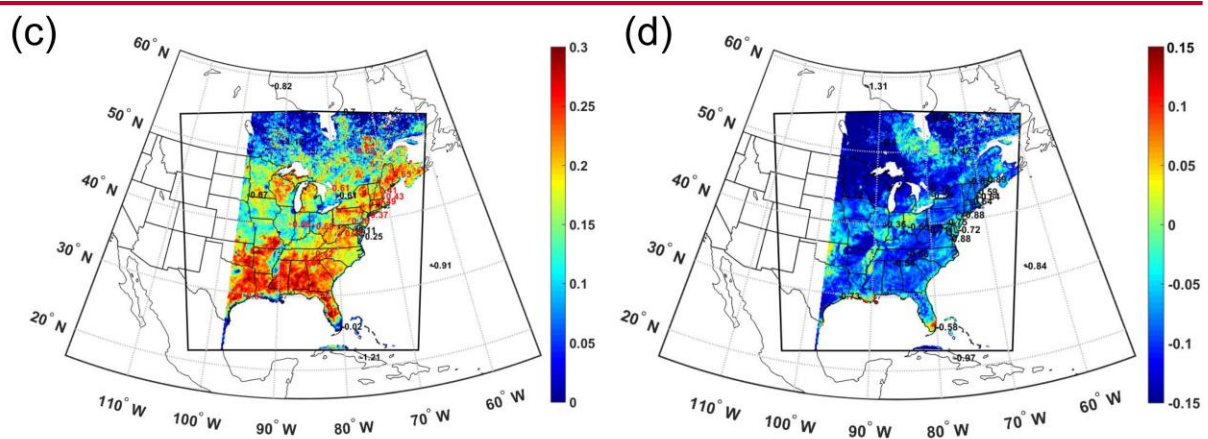
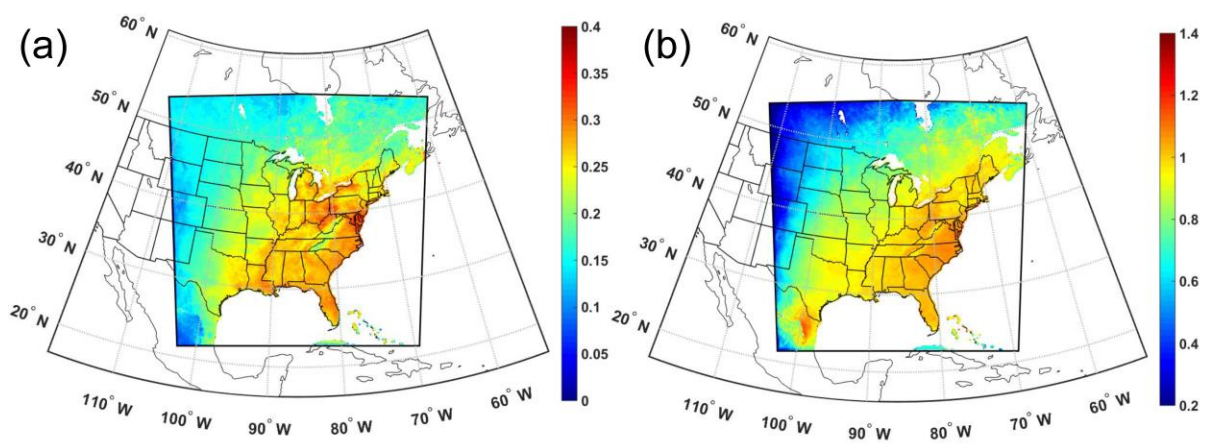
Table 6. Synthesis of the skill with which WRF-Chem identifies the spatial distribution and location of extreme AOD values. Cells with extreme AOD are identified as exceeding the 75th percentile computed on a monthly basis across space from monthly averaged daily means. The second column reports the Accuracy, which indicates the spatial coherence of extremes and non-extremes between WRF-Chem and MODIS. The Accuracy metric is computed as the sum of cells co-identified as exceeding the 75th percentile and not exceeding that threshold by WRF-Chem and MODIS (Terra) relative to the total number of cells with valid data (fifth column, *N*). The third column reports the Threat Score (*TS*) which indicates the probability of correctly forecasting extreme AOD conditional upon either forecasting or observing extremes. The fourth column shows the Hit Rate (*HR*) (i.e. probability of correct forecast), which is the proportion of cells correctly identified as extremes by WRF-Chem relative to MODIS extremes. Values in parenthesis refer to the same metrics when comparing WRF-Chem and MODIS onboard the Aqua satellite.

Month	Accuracy	TS	HR	N
Jan	0.664 (0.651)	0.196 (0.178)	0.328 (0.302)	14899 (15051)
Feb	0.654 (0.583)	0.182 (0.091)	0.308 (0.167)	13721 (13643)
Mar	0.656 (0.647)	0.185 (0.173)	0.312 (0.295)	16641 (16541)
Apr	0.645 (0.680)	0.169 (0.219)	0.289 (0.360)	25265 (24974)
May	0.664 (0.699)	0.196 (0.248)	0.327 (0.397)	32770 (31239)
Jun	0.796 (0.800)	0.420 (0.428)	0.592 (0.600)	36148 (34654)
Jul	0.850 (0.823)	0.538 (0.477)	0.700 (0.646)	36055 (35480)
Aug	0.834 (0.832)	0.500 (0.496)	0.667 (0.663)	39173 (39130)
Sep	0.667 (0.665)	0.200 (0.197)	0.333 (0.329)	35883 (35081)
Oct	0.656 (0.665)	0.185 (0.198)	0.311 (0.330)	29662 (26456)
Nov	0.703 (0.696)	0.254 (0.245)	0.405 (0.393)	21630 (19538)
Dec	0.648 (0.653)	0.173 (0.181)	0.295 (0.306)	14914 (14527)
Mean	0.703 (0.699)	0.266 (0.261)	0.406 (0.399)	26397 (25526)



990 Figure 1. Location of the AERONET stations (colored dots) used in this study and mean daily
991 $\text{PM}_{2.5}$ emissions [$\text{mg m}^{-2} \text{day}^{-1}$] during 2008 (gray shading). Colors indicate the AERONET site
992 classification based on (Kinne et al., 2013): polluted (~~red~~magenta), land (green), coastal (blue),
993 un-classified (yellow). The numbers in panels c-d are MFB for WRF-Chem vs. AERONET

994 stations (red numbers indicate WRF-Chem vs. AERONET has a larger MFB than WRF-Chem
995 vs. MODIS whereas black numbers indicate a lower bias in the comparison with AERONET).



998

999 Figure 2. Mean (a) AOD and (b) AE simulated by WRF-Chem during the year 2008. The mean
1000 values are computed after applying a cloud mask and are for the Terra overpass time. Mean
1001 Fractional Bias (MFB) for (c) AOD and (d) AE for WRF-Chem relative to MODIS (Terra)
1002 (similar results are found for Aqua). ~~The numbers in panels c-d are MFB for WRF-Chem vs~~
1003 ~~AERONET stations (red numbers indicate WRF-Chem vs. AERONET has a larger MFB than~~
1004 ~~WRF-Chem vs. MODIS whereas black numbers indicate a lower bias in the comparison with~~
1005 ~~AERONET).~~ The inner black frame indicates the entire model domain, while as stated in the
1006 text model evaluation is only undertaken for longitudes east of 98°W.

1007

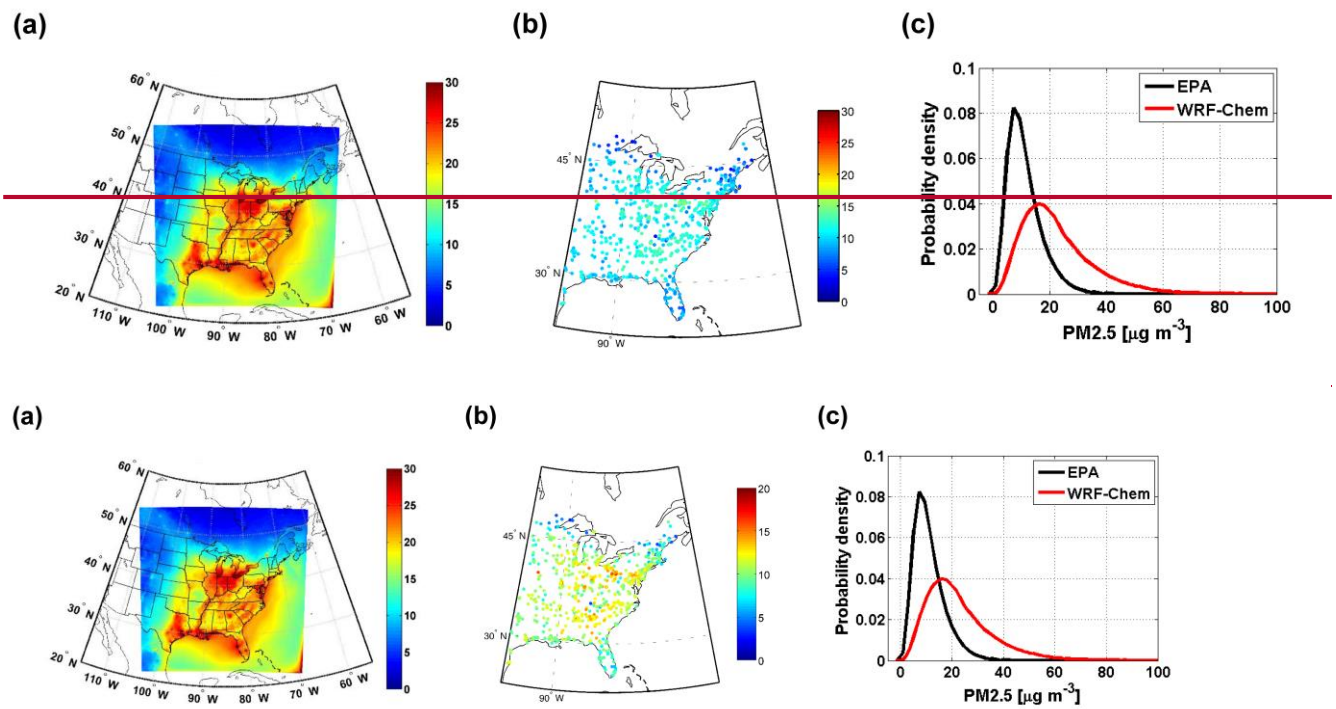


Figure 3. Mean daily PM_{2.5} concentrations [$\mu\text{g m}^{-3}$] during 2008 as (a) simulated by WRF-Chem in the layer closest to the surface and (b) observed at 1230 EPA sites (note the different colorbar). Panel (c) shows the probability distribution of daily mean PM_{2.5} concentrations observed (black line) and simulated (red line) at the measurement stations.

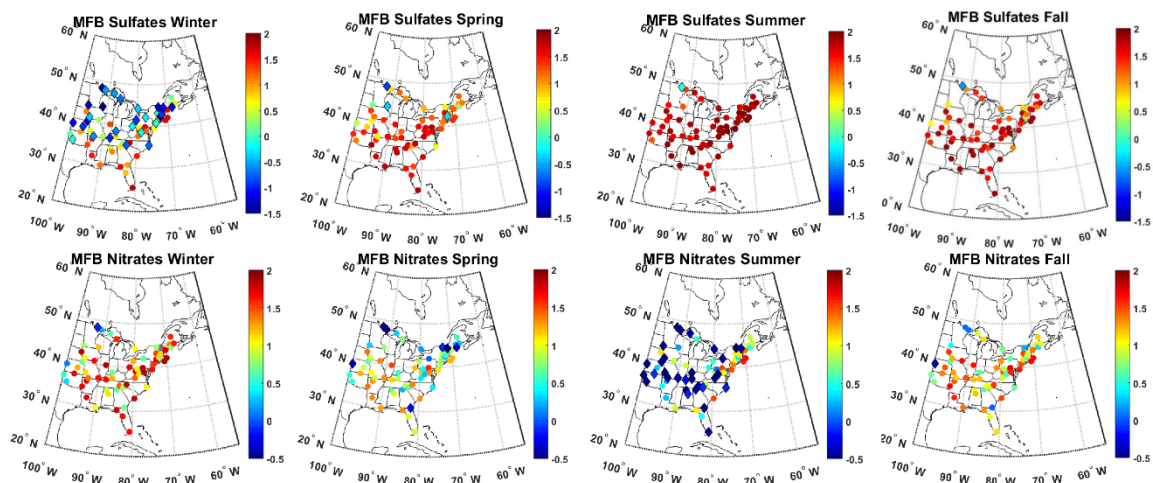
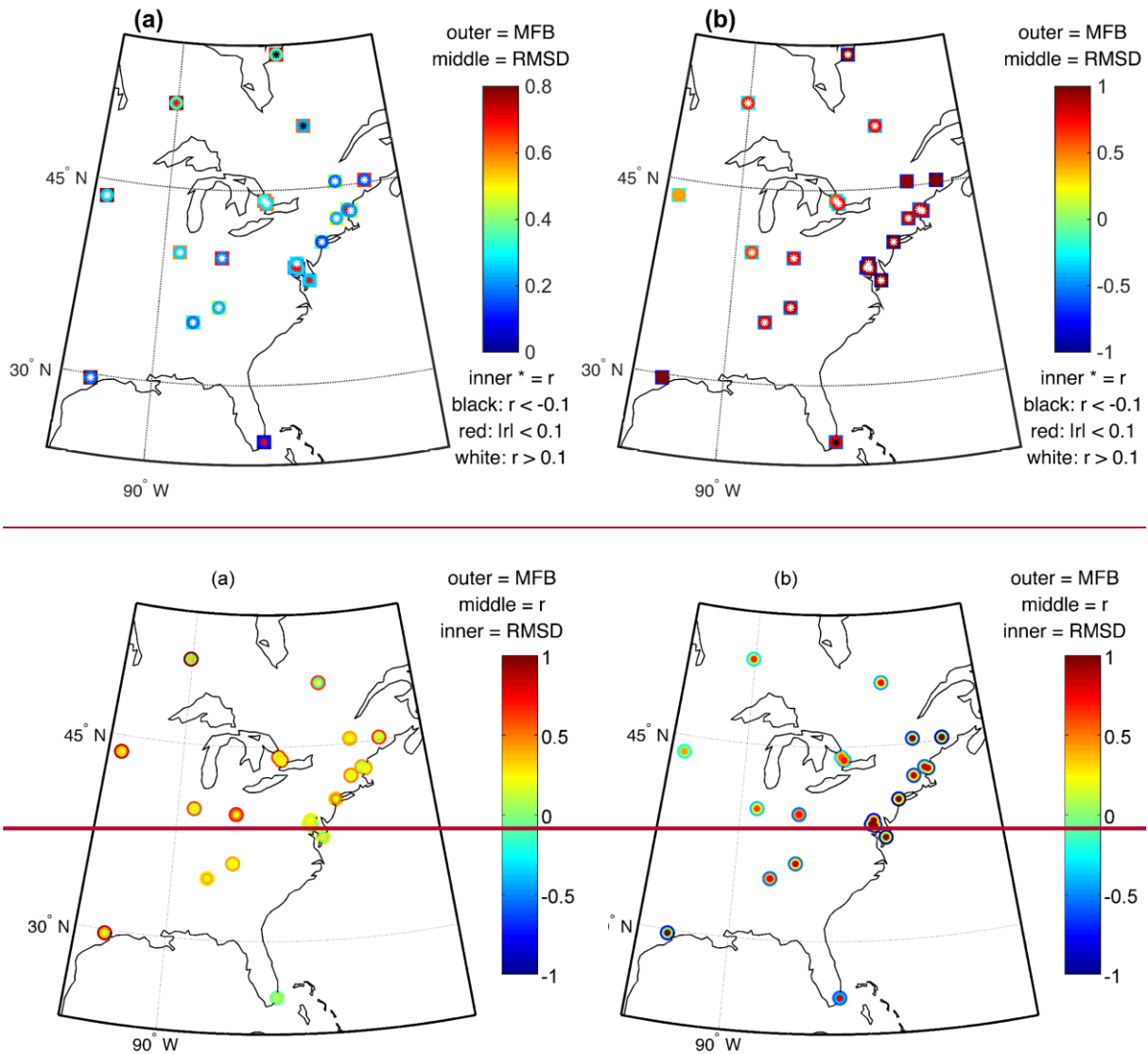


Figure 4. Mean fraction bias (MFB) of near-surface daily mean sulfate (first line) and nitrate (second line) concentrations in fine aerosol particles as simulated by WRF-Chem and observed in PM_{2.5} measurements at 123 IMPROVE sites in different seasons. A positive MFB indicates WRF-Chem overestimates the observations. Note the scales differ between the frames shown for sulfate and nitrate MFB and dots/diamonds refer to positive/negative MFB.

1035

1036



1037

1038

1039

1040 Figure 45. Summary statistics of comparisons of WRF-Chem simulations of (a) AOD and (b)
1041 AE relative to simultaneous observations at the AERONET sites. For a location to be included
1042 in this analysis at least 20 coincident observations and simulations must be available. The
1043 symbols at each AERONET station report MFB (outer ~~circle~~square), root mean squared
1044 difference (RMSD, correlation coefficient (r) (middleinner circle) and correlation coefficient
1045 (r,root mean squared difference (RMSD) (inner *). Note the different colorbar for MFB and
1046 RMSD between the two frames. The correlation coefficient is displayed with different colors

1047 according with 3 classes: $r < -0.1$ (black), $|r| < 0.1$ (red) and $r > 0.1$ (white). ~~Note: For a location~~
1048 ~~to be included in this analysis at least 20 coincident observations and simulations must be~~
1049 ~~available.~~
1050

1051
1052

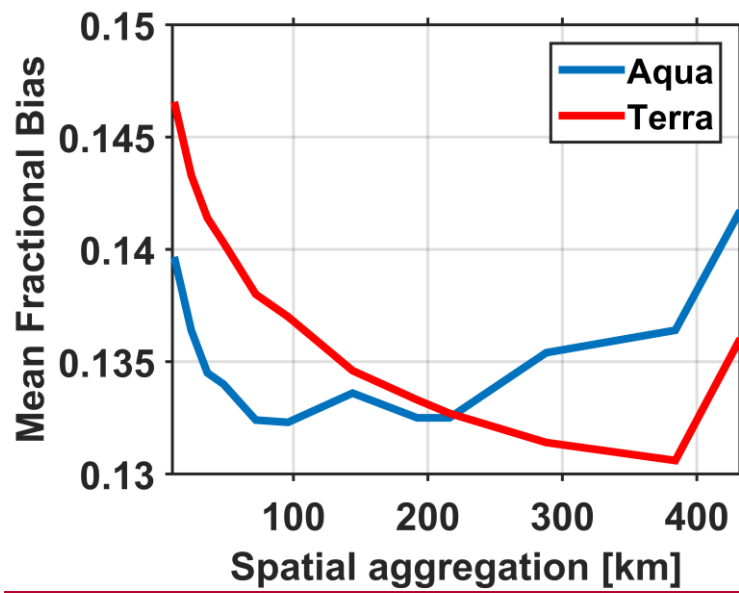


Figure 6. Mean Fractional Bias (MFB) on AOD from WRF-Chem as a function of spatial aggregation relative to observations from Terra (red line) and Aqua (blue line).

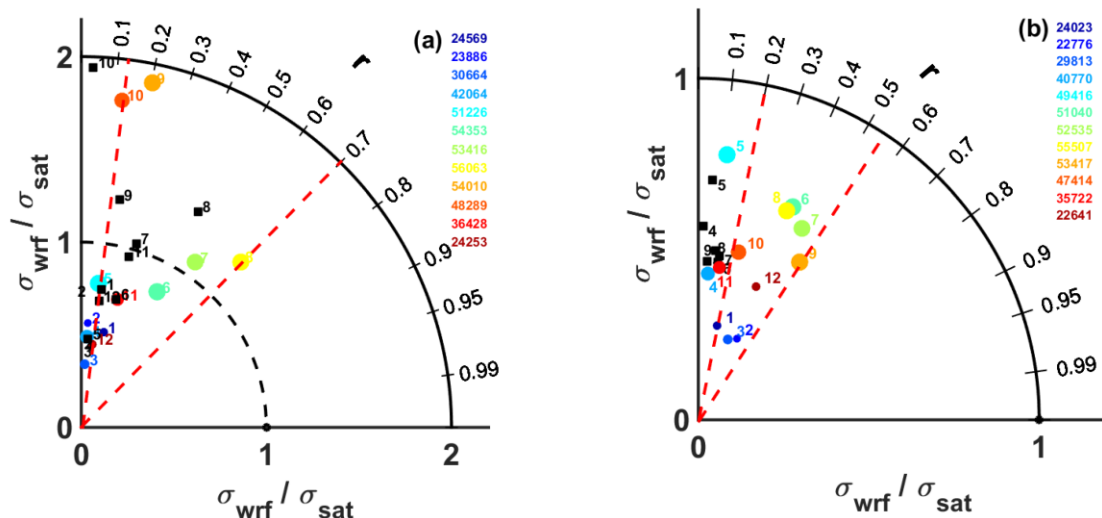


Figure 7. Taylor diagrams comparing the spatial fields of monthly mean (a) AOD and (b) AE from WRF-Chem vs MODIS-Terra (color dots) or MISR (black squares). The numbers shown in the frames denote the month (e.g. 1 = Jan). The numbers shown in the legend indicate the sample size of WRF-Chem data used for computing the monthly mean and the scale of the dots is proportional to the sample size. Note the change in scale for the ratio of standard deviations between the frames. The red dashed lines define the sector with Pearson correlation coefficient between (a) 0.12-0.70 for AOD and (b) 0.20-0.54 for AE which comprise at least two thirds of the months. Each dot/square summarizes the statistics (i.e. RMSD, ratio of standard deviations and correlation coefficient) of the WRF-Chem vs MODIS/MISR comparison for a single month.

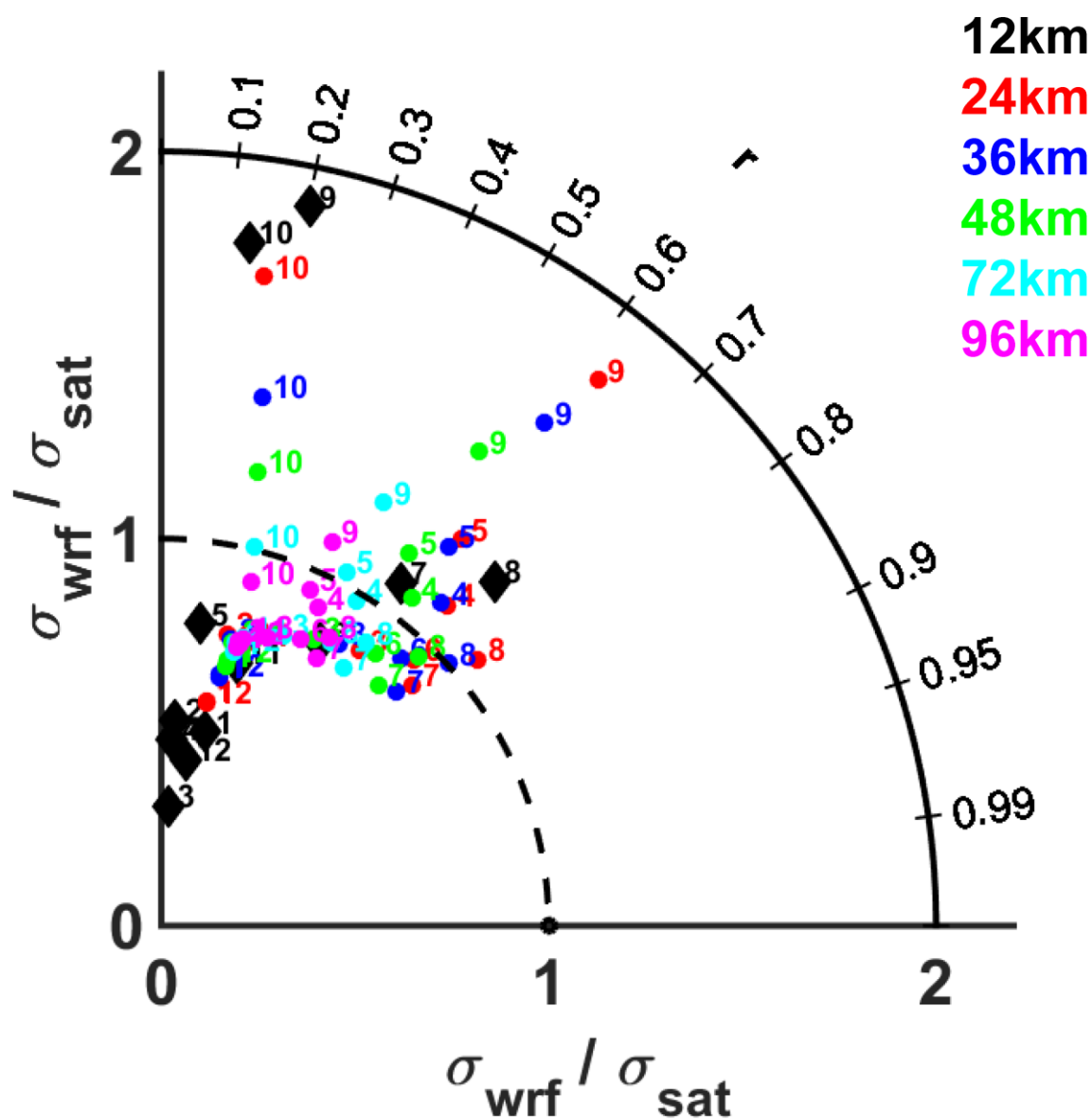


Figure 8. Taylor diagrams for AOD when MODIS observations and WRF-Chem simulations at 12 km are spatially aggregated to 24, 36, 48, 72 and 96 km. Numbers next to the colored dots/diamonds indicate different months (e.g. 1 = Jan).

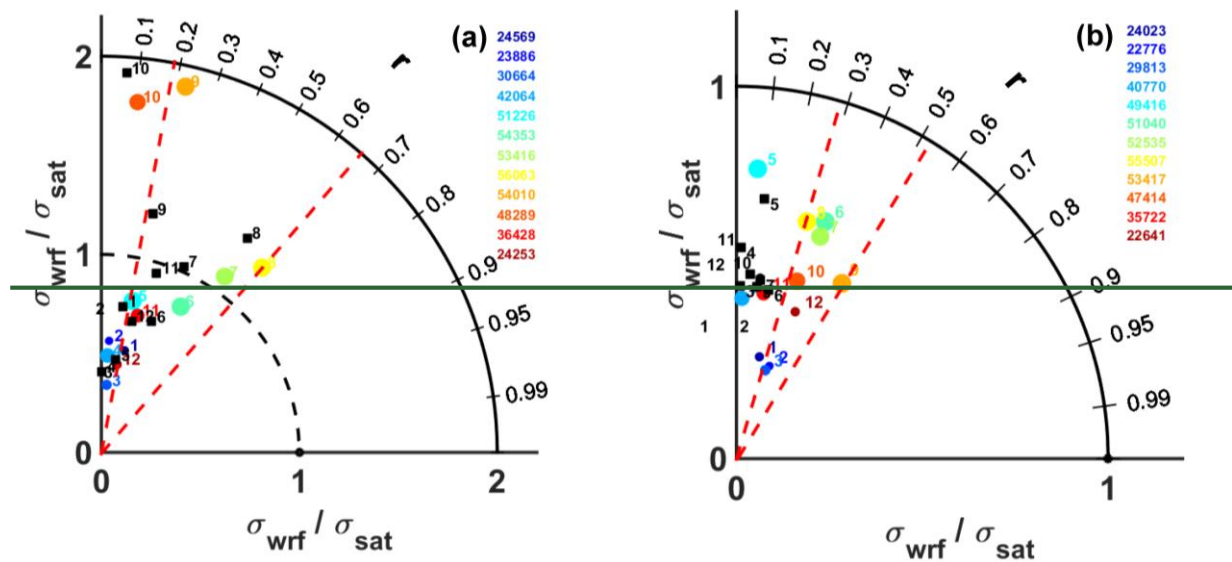


Figure 5. Taylor diagrams comparing the spatial fields of monthly mean (a) AOD and (b) AE from WRF-Chem vs MODIS-Terra (color dots) or MISR (black squares). The numbers shown in the frames denote the month (e.g. 1 = Jan). The numbers shown in the legend indicate the sample size of WRF-Chem data used for computing the monthly mean and the scale of the dots is proportional to the sample size. Note the change in scale for the ratio of standard deviations between the frames. The red dashed lines define the sector with Spearman's rank correlation coefficient between (a) 0.18-0.66 for AOD and (b) 0.28-0.52 for AE which comprise at least two thirds of the months. Each dot/square summarizes the statistics (i.e. RMSD, ratio of standard deviations and correlation coefficient) of the WRF-Chem vs MODIS/MISR comparison for a single month.

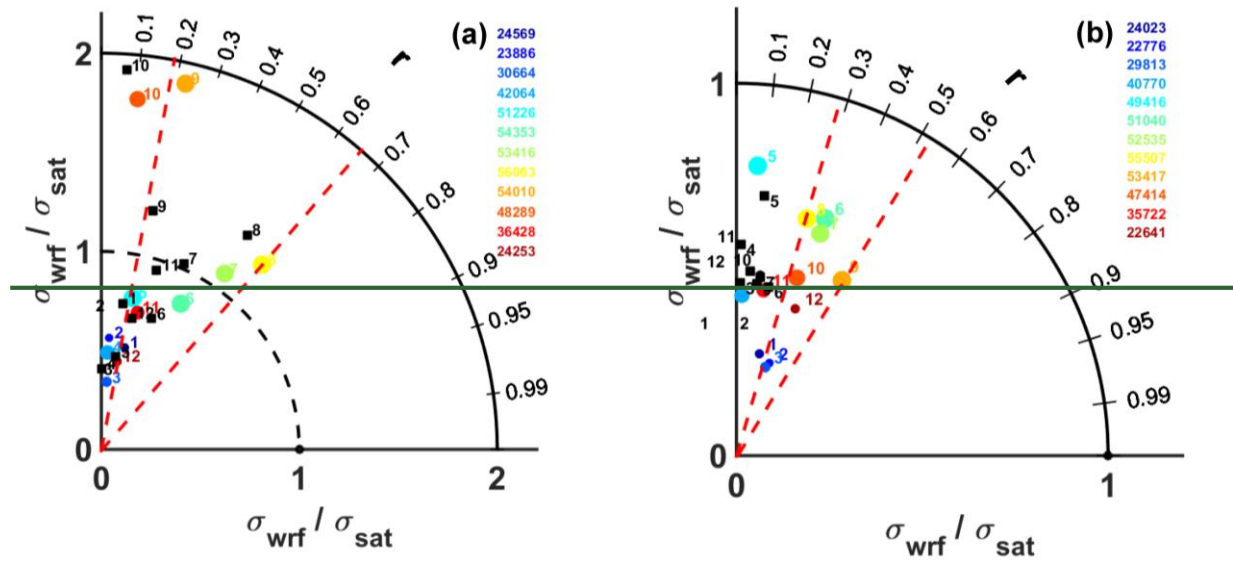


Figure 5. Taylor diagrams comparing the spatial fields of monthly mean (a) AOD and (b) AE from WRF-Chem vs MODIS-Terra (color dots) or MISR (black squares). The numbers shown in the frames denote the month (e.g. 1 = Jan). The numbers shown in the legend indicate the sample size of WRF-Chem data used for computing the monthly mean and the scale of the dots is proportional to the sample size. Note the change in scale for the ratio of standard deviations between the frames. The red dashed lines define the sector with Spearman's rank correlation coefficient between (a) 0.18-0.66 for AOD and (b) 0.28-0.52 for AE which comprise at least two thirds of the months. Each dot/square summarizes the statistics (i.e. RMSD, ratio of standard deviations and correlation coefficient) of the WRF-Chem vs MODIS/MISR comparison for a single month.

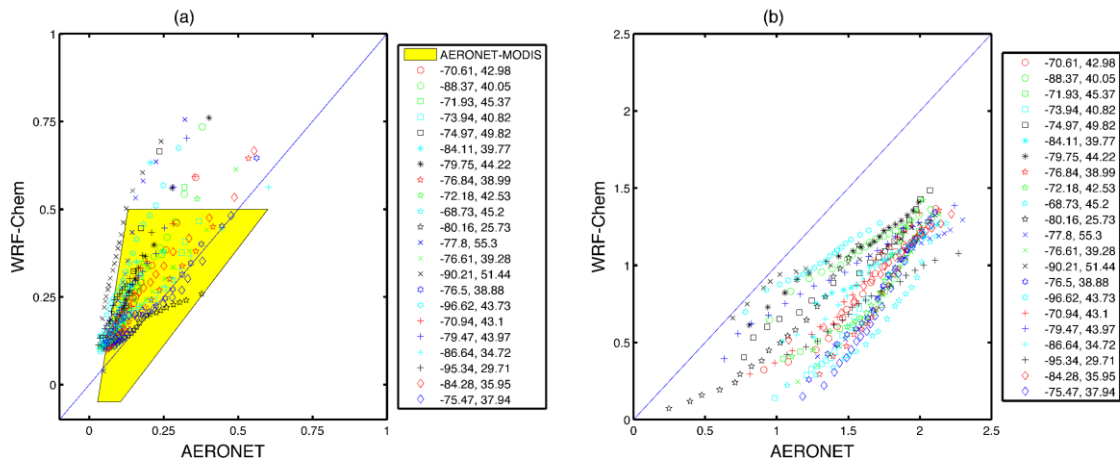


Figure 69. Empirical quantile-quantile (EQQ) plots of (a) AOD and (b) AE of the 5th to 95th percentile as simulated by WRF-Chem relative to 22 AERONET stations (their longitude (E) and latitude (N) is reported in the legend). The yellow shading shows the data envelope for EQQ plots of AERONET and MODIS. For inclusion in the analysis a location must have at least 20 coincident observations and simulations in the grid cell containing the AERONET station. Note MODIS uncertainty in the retrievals (± 0.05) in near zero AOD conditions may lead to negative AOD values which are considered valid. The parameter space for MODIS-AERONET comparisons of AE are not shown because AE from the MODIS L2 data product are strongly bimodal (see examples given in Fig. 1 in the Supplementary Materials).

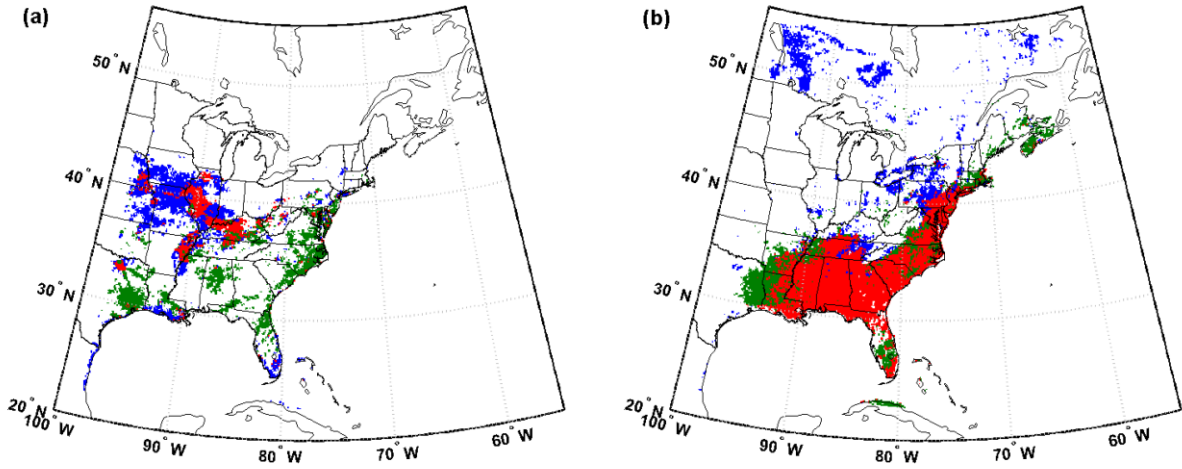
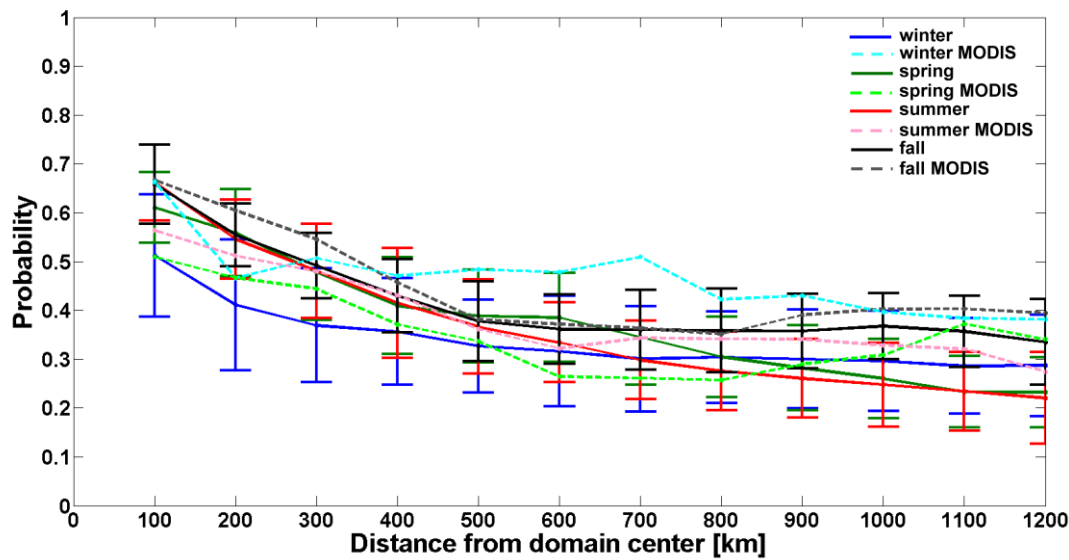


Figure 710. Spatial coherence in extreme AOD (i.e. the occurrence of AOD above the 75th percentile value) from WRF-Chem and MODIS Terra during (a) March (03/2008) and (b) July (07/2008). Green areas denote grid cells defined as experiencing extreme AOD only in the WRF-Chem simulations, blue pixels indicate extreme values as diagnosed using MODIS, while red pixels indicate areas where the occurrence of extreme values is indicated by both the WRF-Chem simulations and the MODIS observations.

1139



1140

1141

1142

1143

1144

1145

1146

1147

1148

1149

Figure 811. Mean and error bars (± 1 standard deviation from the mean) of the probability of co-occurrence of extreme AOD (i.e. AOD > 75th percentile) at the reference location (i.e. domain center) and any other simulated grid cell during different seasons. The distance between the reference point and each grid cell centroid was binned using 100 km distance classes. Solid lines indicate mean seasonal spatial scales simulated by WRF-Chem, whereas dashed lines are observed means from L2 MODIS data (only the mean of the coherence ratios is plotted for the MODIS data).